Inorg. Chem. **2007**, *46*, 8638–8651

Synthesis, Structure, Spectroscopic Properties, and Electrochemical Oxidation of Ruthenium(II) Complexes Incorporating Monocarboxylate Bipyridine Ligands

Nickita Nickita,[†] Matthew J. Belousoff,[†] Anand I. Bhatt,[†,‡] Alan M. Bond,[†] Glen B. Deacon,[†] Gilles Gasser,[†] and Leone Spiccia*[,†]

School of Chemistry and Centre for Green Chemistry, Monash University, Victoria 3800, Australia

Received April 26, 2007

$[Ru(bpy)_2(Mebpy\text{-}COOH)](PF_6)_2\cdot 3H_2O$ (**1**), $[Ru(phen)_2(Mebpy\text{-}COOH)](ClO_4)_2\cdot 5H_2O$ (**2**), $[Ru(dppz)_2(Mebpy\text{-}COOH)]Cl_2\cdot 9H_2O$ (**3**), and $[Ru(bpy)(dppz)(Mebpy\text{-}COOH)](PF_6)_2\cdot 5H_2O$ (**4**) (bpy = 2,2′-bipyridine, Mebpy-COOH = 4′-methyl-2,2′-bipyridine-4-carboxylic acid, phen = 1,10-phenanthroline, dppz = dipyrido[3,2,-a;2′,3-c]phenazine) have been synthesized and characterized spectroscopically and by microanalysis. The $[Ru(Mebpy\text{-}COOH)(CO)_2Cl_2]\cdot H_2O$ intermediate was prepared by reaction of the monocarboxylic acid ligand, Mebpy-COOH, with $[Ru(CO)_2Cl_2]_n$, and the product was then reacted with either bpy, phen, or dppz in the presence of an excess of trimethylamine-*N*-oxide (Me_3NO), as the decarbonylation agent, to generate **1**, **2**, and **3**, respectively. For compound **4**, $[Ru(bpy)(CO)Cl_2]_2$ was reacted with Mebpy-COOH to yield $[Ru(bpy)(Mebpy\text{-}COOH)(CO)Cl](PF_6)\cdot H_2O$ as a mixture of two main geometric isomers. Chemical decarbonylation in the presence of dppz gave **4** also as a mixture of two isomers. Electrochemical and spectrophotometric studies indicated that complexes **1** and **2** were present as a mixture of protonated and deprotonated forms in acetonitrile solution because of water of solvation in the isolated solid products. The X-ray crystal structure determination on crystals of $[Ru(bpy)_2(MebpyCOO)][Ru(bpy)_2(Mebpy\text{-}COOH)]_3(PF_6)_7$, **1a**, and $[Ru(phen)_2(MebpyCOO)](ClO_4)\cdot 6H_2O$, **2a**, obtained from solutions of **1** and **2**, respectively, revealed that **1a** consisted of a mixture of protonated and deprotonated forms of the complex in a 1:3 ratio and that **2a** consisted of the deprotonated derivative of **2**. A distorted octahedral geometry for the Ru^{II} centers was found for both complexes. Upon excitation at 450 nm, MeCN solutions of the protonated complexes **1**–**4** were found to exhibit emission bands in the 635-655 nm range, whereas the corresponding emission maxima of their deprotonated forms were observed at lower wavelengths. Protonation/deprotonation effects were also observed in the luminescence and electrochemical behavior of complexes **1**–**4**. Comprehensive electrochemical studies in acetonitrile show that the ruthenium centers on **1**, **2**, **3**, and **4** are oxidized from Ru^{II} to Ru^{III} with reversible potentials at 917, 929, 1052, and 1005 mV vs $Fc^{0/+}$ (Fc = ferrocene), respectively. Complexes **1** and **2** also exhibit an irreversible oxidation process in acetonitrile, and all compounds undergo ligand-based reduction processes.

Introduction

Since the luminescent properties of $[Ru(bpy)_3]^{2+}$ (bpy = 2,2′-bipyridine) were first reported by Paris and Brandt,[1] tris-(diimine) and related Ru complexes have been investigated extensively. For example, the use of these complexes as photosensitizers for the conversion of light (solar) energy to chemical or electrical energy has received considerable attention.[2] In particular, an area of significant interest lies in the design and optimization of dye-sensitized solar cells (DSSCs), whereby functionalized Ru^{II} complexes are bound onto TiO_2-electrode surfaces.[2−4] The long-lived excited-state lifetimes and characteristic redox behavior has, more recently, led to the use of ruthenium(II) complexes as molecular probes for bioconjugates.[5−8]

* To whom correspondence should be addressed. E-mail: Leone.Spiccia@sci.monash.edu.au. Fax: +61 3 9905 4597. Phone: +61 3 9905 4526.

[†] School of Chemistry.

[‡] Centre for Green Chemistry.

(1) Paris, J. P.; Brandt, W. W. *J. Am. Chem. Soc.* **1959**, *81*, 5001−5002.

(2) Gratzel, M. *Coord. Chem. Rev.* **1991**, *111*, 167−174 and references therein.

(3) Kalyanasundaram, K. *Coord. Chem. Rev.* **1982**, *46*, 159−244 and references therein.

(4) Nazeeruddin, M. K.; Klein, C.; Liska, P.; Gratzel, M. *Coord. Chem. Rev.* **2005**, *249*, 1460−1467 and references therein.

10.1021/ic700796m CCC: $37.00
Published on Web 09/20/2007

Scheme 1. Synthesis of Bis and Tris Heteroleptic Complexes via Decarbonylation[9,30−36]

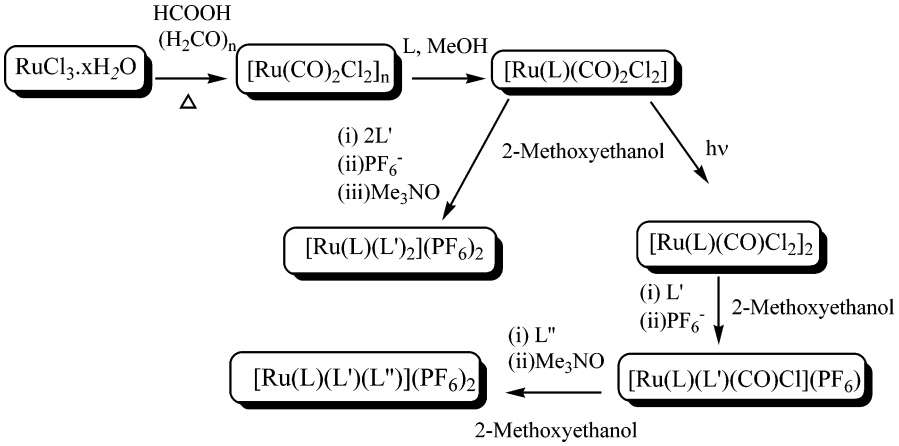

Since the light absorption and redox properties of the Ru^{II} center can be tuned through variation of the ligands, complexes with different poly(imine) ligands have been synthesized and investigated.[9] In particular, many $[Ru(L)_3]^{2+}$, $[Ru(L)_2(L')]^{2+}$, $[Ru(L)_2(X_2)]^{2+}$, $[Ru(L)(L')(L'')]^{2+}$ (L, L′, L″ = bidentate diimine ligand, X = neutral monodentate ligand), $[Ru(L)(X)_3]^{3+}$, $[Ru(L)_2]^{3+}$, and $[Ru(L)(L')]^{2+}$ (L, L′ = tridentate triimine ligands, X = neutral monodentate ligand) complexes have been prepared, and their physicochemical properties have been investigated.[9] These types of complexes have attracted interest as multielectron-transfer catalysts,[10,11] fluorescent[12,13] and electrochemical anion sensors,[14,15] molecular devices and machines,[16,17] reagents for reduction of carbon dioxide to carbon monoxide and formate,[18−20] and catalysts for the water−gas shift reaction.[3]

Several routes for the synthesis of heteroleptic ruthenium(II) complexes have previously been reported.[9] For example, $[Ru(DMSO)_4Cl_2]$ and $[Ru(C_6H_6)Cl_2]_2$ have been used as precursors for ruthenium(II) tris(diimine) complexes.[21,22] A major synthetic methodology to tris(diimine) complexes bearing carboxylate functionalities for various applications has involved the use of $[Ru(bpy)_2Cl_2]$, $[Ru(phen)_2Cl_2]$, or $[Ru(L)_2Cl_2]$ (L = diimine ligand) as the starting reagent.[23−29] An alternative methodology leading to the formation of heteroleptic bis- and tris-(diimine)ruthenium(II) complexes involves halide bridge splitting combined with chemical or photochemical decarbonylation of the $[Ru(CO)_2Cl_2]_n$ precursor and intermediate complexes (see Scheme 1).[9,30−33] The first reaction step toward both types of complexes involves the addition of a bidentate diimine ligand, L, to $[Ru(CO)_2Cl_2]_n$.[34−36] This results in the formation of $[Ru(L)(CO)_2Cl_2]$, which can then be reacted with two molecules of the next bidentate diimine ligand, L′, to form $[Ru(L)(L')_2]^{2+}$.[34,35] This decarbonylation step involves the

(5) Verheijen, J. C.; Van der Marel, G. A.; Van Boom, J. H.; Metzler-Nolte, N. *Bioconjugate Chem.* **2000**, *11*, 741−743.
(6) Khan, S. I.; Beilstein, A. E.; Grinstaff, M. W. *Inorg. Chem.* **1999**, *38*, 418−419.
(7) Telser, J.; Cruickshank, K. A.; Schanze, K. S.; Netzel, T. L. *J. Am. Chem. Soc.* **1989**, *111*, 7221−7226.
(8) Mitra, D.; Di Cesare, N.; Sleiman, H. F. *Angew. Chem., Int. Ed.* **2004**, *43*, 5804−5808.
(9) Spiccia, L.; Deacon, G. B.; Kepert, C. M. *Chem. Coord. Rev.* **2004**, *248*, 1329−1341 and references therein.
(10) Balzani, V.; Scandola, F. *Supramolecular Photochemistry*; Horwood: Chichester, U.K., 1991.
(11) Nagashima, H.; Kondo, H.; Hayashida, T.; Yamaguchi, Y.; Gondo, M.; Masuda, S.; Miyazaki, K.; Matsubara, K.; Kirchner, K. *Coord. Chem. Rev.* **2003**, *245*, 177−190 and references therein.
(12) Szemes, F.; Hesek, D.; Chen, Z.; Dent, S. W.; Drew, M. G. B.; Goulden, A. J.; Graydon, A. R.; Grieve, A.; Mortimer, R. J.; Wear, T.; Weightman, J. S.; Beer, P. D. *Inorg. Chem.* **1996**, *35*, 5868−5879.
(13) Vickers, M. S.; Martindale, K. S.; Beer, P. D. *J. Mater. Chem.* **2005**, *15*, 2784−2790.
(14) Beer, P. D.; Szemes, F.; Balzani, V.; Sala, C. M.; Drew, M. G. B.; Dent, S. W.; Maestri, M. *J. Am. Chem. Soc.* **1997**, *119*, 11864−11875.
(15) Beer, P. D.; Hayes, E. J. *Coord. Chem. Rev.* **2003**, *240*, 167−189 and references therein.
(16) Balzani, V.; Juris, A.; Venturi, M. *Coord. Chem. Rev.* **1996**, *96*, 759−833 and references therein.
(17) Balzani, V.; Bergamini, G.; Marchioni, F.; Ceroni, P. *Coord. Chem. Rev.* **2006**, *250*, 1254−1266 and references therein.
(18) Ishida, H.; Tanaka, K.; Tanaka, T. *Organometallics* **1987**, *6*, 181−186.
(19) Lehn, J. M.; Ziessel, R. J. *J. Organomet. Chem.* **1990**, *382*, 157−173.
(20) Tanaka, K.; Ooyama, D. *Coord. Chem. Rev.* **2002**, *226*, 211−218 and references therein.
(21) Zakeeruddin, S. M.; Nazeeruddin, M. K.; Humphrey-Baker, R.; Gratzel, M. *Inorg. Chem.* **1998**, *37*, 5251−5259.
(22) Maxwell, K. A.; Sykora, M.; De Simone, J. M.; Meyer, T. J. *Inorg. Chem.* **2000**, *39*, 71−75.
(23) Peek, B. M.; Ross, G. T.; Edwards, S. W.; Meyer, G. J.; Meyer, T. J.; Erickson, B. W. *J. Pep. Protein Res.* **1991**, *38*, 114−123.
(24) Uppadine, L. H.; Keene, F. R.; Beer, P. D. *J. Chem. Soc. Dalton Trans.* **2001**, *14*, 2188−2198.
(25) Shan, B.-Z.; Zhao, Q.; Goswami, N.; Eichhorn, D. M.; Rillema, D. P. *Coord. Chem. Rev.* **2001**, *211*, 117−144.
(26) Zhou, M.; Robertson, G. P.; Roovers, J. *Inorg. Chem.* **2005**, *44*, 8317−8325.
(27) Ogawa, M.; Wishart, J. F.; Young, Z.; Miller, J. R.; Iised, S. S. *J. Phys. Chem.* **1993**, *97*, 11456−11463.
(28) Lintuluoto, J. M.; Borovkov, V. V.; Inoue, Y. *Tetrahedron Lett.* **2000**, *41*, 4781−4786.
(29) Zheng, G. Y.; Wang, Y.; Rillema, D. P. *Inorg. Chem.* **1996**, *35*, 7118−7123.
(30) Deacon, G. B.; Kepert, C. M.; Sahely, N.; Skelton, B. W.; Spiccia, L.; Thomas, N. C.; White, A. H. *J. Chem. Soc., Dalton Trans.* **1999**, 275−277.
(31) Black, D. S. C.; Deacon, G. B.; Thomas, N. C. *Aust. J. Chem.* **1982**, *35*, 2445-2453.
(32) Kepert, C. M.; Bond, A. M.; Deacon, G. B.; Spiccia, L.; Skelton, B. W.; White, A. H. *J. Chem. Soc., Dalton Trans.* **2004**, 1766−1774.
(33) Kepert, C. M.; Deacon, G. B.; Sahely, N.; Spiccia, L.; Fallon, G. D.; Skelton, B. W.; White, A. H. *Inorg. Chem.* **2004**, *43*, 2818−2827.
(34) Thomas, N. C.; Deacon, G. B. *Inorg. Synth.* **1989**, *25*, 107−110.
(35) Black, D. S. C.; Deacon, G. B.; Thomas, N. C. *Inorg. Chim. Acta.* **1982**, *65*, L75−L76.
(36) Anderson, P. A.; Deacon, G. B.; Haarmann, K. H.; Keene, F. R.; Meyer, T. J.; Reitsma, D. A. N.; Skelton, B. W.; Strouse, G. F.; Thomas, N. C.; Treadway, J. A.; White, A. H. *Inorg. Chem.* **1995**, *34*, 6145−6157.

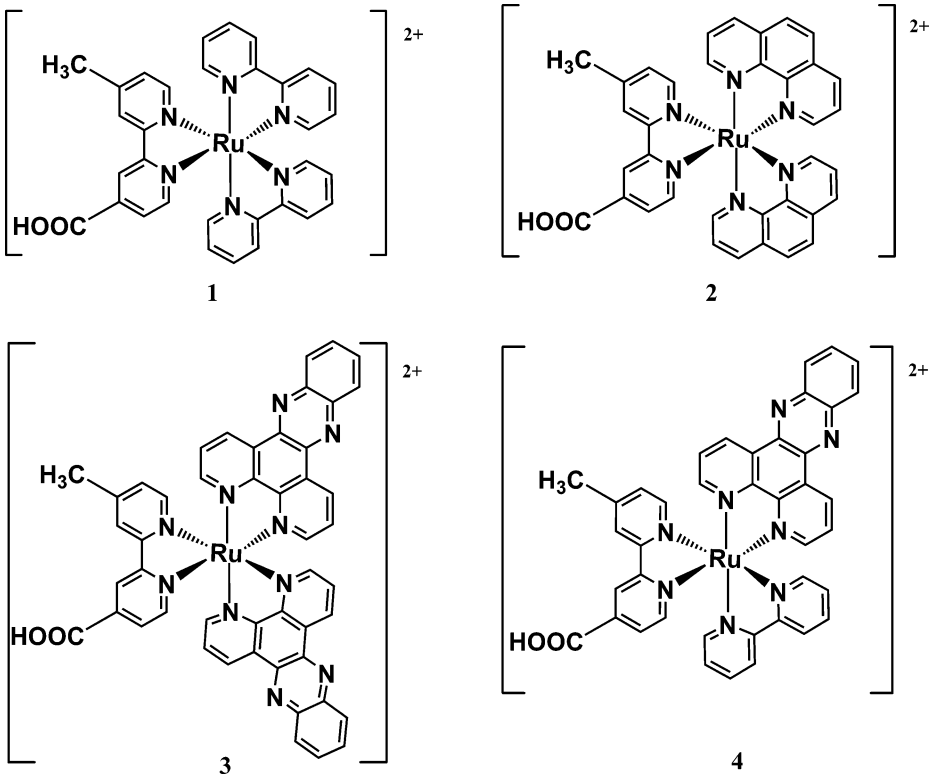

Figure 1. Structures of **1**−**4**.

direct substitution of both the chloro and carbonyl ligands in $[Ru(L)(CO)_2Cl_2]$ by the second ligand to obtain the final product. In the route to tris(heteroleptic) complexes (Scheme 1), $[Ru(L)(CO)_2Cl_2]$ undergoes photochemical decarbonylation upon irradiation with visible light to form $[Ru(L)(CO)Cl_2]_2$.[30] This dimer then undergoes bridge splitting upon addition of a second bidentate diimine ligand, L′, to form $[Ru(L)(L')(CO)Cl]^+$.[32,33] In the final step, chemical decarbonylation of $[Ru(L)(L')(CO)Cl]^+$ by trimethylamine-*N*-oxide (Me_3NO) in the presence of another bidentate diimine ligand (L″) affords the desired heteroleptic tris-(diimine)-ruthenium(II) complex.[32]

Until now, these decarbonylation routes have generally been used to prepare ruthenium(II) complexes of alkyl-substituted or unsubstituted diimine ligands. We demonstrate here that the decarbonylation methodology provides an efficient way of preparing ruthenium(II) complexes of carboxylate-functionalized diimine ligands. The synthesis and spectroscopic characterization of four ruthenium(II) complexes of the monocarboxylate diimine ligand, Mebpy-COOH (**1**−**4**, see Figure 1) are reported. The single carboxylate moiety on this ligand allows further functionalization of the Ru^{II} complexes to take place, for example, in the development of nucleic acid derivatives and bioconjugates such as those reported by Metzler-Nolte et al.[5,37] and Achim et al.[38,39] Metzler-Nolte and co-workers first attached $[Ru(bpy)_2(Mebpy\text{-}COOH)]^{2+}$ (**1**) to the N-terminus of a thymine PNA monomer[37] and then incorporated **1** into a PNA heptamer via automated synthesis.[5]

In the case of **3** and **4**, we have introduced a ligand, dppz, that is known to intercalate into biomolecules such as RNA and DNA since similar metal intercalating conjugates exhibit enhanced luminescence behavior.[40,41] Although **1** and **2** have been prepared from $[Ru(bpy)_2Cl_2]$ and $[Ru(phen)_2Cl_2]$,[23,26−28,42] the luminescence and electrochemistry of these complexes were not described in detail. Compounds **1**−**4** have been characterized using ^1H NMR spectroscopy, UV−vis spectrophotometry, emission spectroscopy, electrochemistry, and in the case of $[Ru(bpy)(MebpyCOO)][Ru(bpy)_2(Mebpy\text{-}COOH)]_3(PF_6)_7$, **1a**, and $[Ru(phen)_2(MebpyCOO)](ClO_4)\cdot 6H_2O$, **2a**, single-crystal X-ray diffraction.

Experimental Section

Chemicals. $RuCl_3\cdot xH_2O$ (Pressure Chemicals) and 4,4′-dimethyl-2,2′-bipyridine (GFS Chemicals) were used as supplied. Other chemicals obtained from commercial suppliers were of reagent or analytical grade and were used without further purification. 4′-Methyl-2,2′-bipyridine-4-carboxylic acid and dipyrido[3,2,-a;2′,3-c]phenazine were synthesized by literature procedures.[23,43] HPLC-grade MeCN (Merck) was used for all spectral and electrochemical studies. Tetrabutylammonium hexafluorophosphate ($^nBu_4NPF_6$, Fluka) was recrystallized prior to use as the electrolyte for the electrochemical studies in MeCN.[44]

(37) Hess, A.; Metzler-Nolte, N. *Chem. Commun.* **1999**, 885−886.
(38) Franzini, R. M.; Watson, R. M.; Patra, G. K.; Breece, R. M.; Tierney, D. L.; Hendrich, M. P.; Achim, C. *Inorg. Chem.* **2006**, *45*, 9798−9811.
(39) Popescu, D.-L.; Parolin, T. J.; Achim, C. *J. Am. Chem. Soc.* **2003**, *125*, 6354−6355.
(40) Bhattarcharya, P. K.; Barton, J. K.; Delaney, S.; Paschaly, M. *Inorg. Chem.* **2002**, *41*, 1966−1974.
(41) Erkkila, K. E.; Odom, D. T.; Barton, J. K. *Chem. Rev.* **1999**, *99*, 2777−2796.
(42) Crean, C. W.; Kavanagh, Y. T.; O'Keeffe, C. M.; Lawler, M. P.; Stevenson, C.; Davies, R. J. H.; Boyle, P. H.; Kelly, J. M. *Photochem. Photobiol. Sci.* **2002**, *1*, 1024−1033.
(43) Dickeson, J. E.; Summers, L. A. *Aust. J. Chem.* **1970**, *23*, 1023−1027.

Instrumentation and Methods. Thin layer chromatography (TLC) was performed using silica gel 60 F-254 (Merck) plates, followed by preparative column chromatography on silica gel. ^{1}H NMR and ^{1}H−^{1}H COSY spectra were recorded on either 300 or 400 MHz Bruker NMR spectrometers. The chemical shifts, δ, were calibrated using either tetramethylsilane (TMS) or signals from the residual protons of the deuterated solvents. UV−vis spectra were recorded on a Varian Cary 3 or Cary 5G spectrophotometer. Luminescence emission spectra were obtained following excitation at 450 nm using a Varian fluorescence spectrometer equipped with a 250 W xenon lamp as an excitation source. Spectra were absorbance matched and corrected for variations in PMT response. These measurements were carried out in acetonitrile at room temperature using complex concentrations of 0.01−1 mM. IR spectra measured on KBr disks were recorded with a Perkin-Elmer FTIR 1600 series spectrometer at a resolution of 4 cm^{-1}. Mass spectra were recorded using a Micromass Platform II instrument with an ESI source. The capillary voltage was set at 3.5 eV, and the cone voltage was set at at 35 V. Elemental analysis was performed by the Campbell Microanalytical Laboratory, University of Otago, New Zealand.

Electrochemical Measurements. Voltammetric measurements in acetonitrile were performed over the scan rate range of 0.002−1 V s^{-1},[45] using either a BAS100 (Bioanalytical Systems) or a VoltaLab PGZ301 (Radiometer Analytical) electrochemical workstation. Oxygen was removed from the acetonitrile solutions by purging the solutions with high-purity nitrogen. A typical three-electrode cell was employed which was composed of a glassy carbon (0.0096 cm^2) or platinum working electrode (0.0079 cm^2), a large surface area Pt counter electrode, and an Ag/$AgNO_3$/MeCN (0.1 M $AgNO_3$) reference electrode. A large platinum disk electrode (0.071 cm^2) was also used in the cyclic voltammetric experiments. Rotating disc voltammetry at rates from 500 to 3000 rpm used a platinum disk working electrode (0.071 cm^2), and rotations were carried out with a Metrohm 628-10 system. The potential of the reference electrode was calibrated against the ferrocene/ferrocenium (Fc/Fc^+) redox couple by monitoring the reversible potential for oxidation of ferrocene under the conditions used to carry out the voltammetry of the ruthenium(II) complexes. All electrochemical experiments were carried out at 293 ± 2 K inside a Faraday cage under a nitrogen atmosphere and with 0.1 M of Bu_4NPF_6 in MeCN as the supporting electrolyte. The working electrodes were polished with an aqueous aluminum oxide slurry (0.3 μm); then they were rinsed with acetone and dried before each voltammetric experiment. Controlled potential bulk electrolysis experiments were carried out under a nitrogen atmosphere at a large surface area Pt gauze basket working electrode using 0.05−2.0 mM concentrations of **1**−**4**. In these bulk electrolysis experiments, both the working and the reference electrodes were separated from the solvent (electrolyte) solution containing the Pt gauze basket counter electrode by a glass frit. Electrolysis was assumed to be complete when the charge passed per minute was less than 1% of the charge passed in the first minute. ***Caution!*** Transition metal perchlorates are potentially explosive and should be prepared in small quantities and handled with care.

$[Ru(CO)_2Cl_2]_n$, $[Ru(bpy)(CO)_2Cl_2]$ and $[Ru(bpy)(CO)Cl_2]_2$. These compounds were prepared via literature methods.[30,31,36] The IR spectra of these compounds and ^{1}H NMR spectrum for $[Ru(bpy)(CO)_2Cl_2]$ were in agreement with the literature reports.[30,31,36]

***cis*-Dicarbonyl-*trans*-dichloro(4′-methyl-2,2′-bipyridine-4-carboxylic acid)ruthenium(II) hydrate, $[Ru(Mebpy\text{-}COOH)(CO)_2Cl_2]\cdot H_2O$.** $[Ru(CO)_2Cl_2]_n$ (0.50 g, 2.8 mmol) was suspended in 25 mL of methanol under a stream of nitrogen and 4′-methyl-2,2′-bipyridine-4-carboxylic acid (0.71 g, 3.2 mmol) was added. The mixture was refluxed at 60 °C for 20 min. This resulted in the dissolution of $[Ru(CO)_2Cl_2]_n$, followed by precipitation of the product. The mixture was then cooled to 2 °C to complete the precipitation. A pale yellow product was collected, washed with cold methanol, and dried in a vacuum desiccator (yield 0.76 g, 62%).

Characterization Data. Anal. Found (%): C, 36.9; H, 2.8; N, 6.0. Calcd for $C_{14}H_{12}Cl_2N_2O_5Ru$ (%): C, 36.5; H, 2.6; N, 6.1. IR bands (KBr, ν/cm^{-1}): 2077 s, 2003 s, 1723 m, 1619 w, 1559 w, 1485 w, 1407 m, 1384 w, 1304 m, 1237 m, 1126 w, 1035 m, 832 w, 771 w. ^{1}H NMR (acetone-d_6): δ 9.43 (d, 1H, H6, ^3J = 5.6 Hz), 9.10 (d, 1H, H6′, ^3J = 5.7 Hz), 9.01 (s, 1H, H3), 8.81 (s, 1H, H3′), 8.30 (dd, 1H, H5, ^3J = 5.9 Hz, ^4J = 6.5 Hz), 7.73 (m, 1H, H5′), 2.70 (s, 3H, CH_3). Electrospray mass spectrum (*m*/*z*) (positive mode): 442 [$(Ru(Mebpy\text{-}COOH)(CO)_2Cl_2)^+$, $(M)^+$].

Bis(2,2′-bipyridine)(4′-methyl-2,2′-bipyridine-4-carboxylic acid)ruthenium(II) hexafluorophosphate trihydrate, $[Ru(bpy)_2(Mebpy\text{-}COOH)](PF_6)_2\cdot 3H_2O$ (1). 2,2′-Bipyridine (0.20 g, 1.3 mmol) and an excess of Me_3NO (0.39 g, 5.2 mmol) were added to a solution of $[Ru(Mebpy\text{-}COOH)(CO)_2Cl_2].H_2O$ in deoxygenated 2-methoxyethanol (0.51 g, 1.2 mmol in 25 mL). This solution was refluxed at 120 °C for 3 h. After the solution was cooled to room temperature, the solvent was removed via rotary evaporation, and the crude product was purified by column chromatography on silica gel (eluent MeCN/H_2O/aqueous saturated solution of KNO_3, 10:3:1 v/v). The darkest band was collected, and solvent was removed under reduced pressure. The residue was suspended in MeCN to dissolve the complex and to separate it from the insoluble KNO_3. After filtration, MeCN was removed via rotary evaporation, and the product was redissolved in 5 mL of water; 1 M KPF_6 solution was added dropwise, until no further precipitation was observed, to give dark red microcrystals. The crystals were collected by filtration, washed with ether, and dried under high vacuum to give **1** as a dark red solid (yield 0.39 g, 36%). Crystals of **1a** suitable for X-ray crystallography were obtained by slow evaporation of a mixture of acetonitrile and water containing **1** and KPF_6 and consisted of a 1:3 mixture of the deprotonated $[Ru(bpy)_2(Mebpy\text{-}COO)]^+$ and protonated $[Ru(bpy)_2(Mebpy\text{-}COOH)]^{2+}$ complexes.

Characterization Data for 1. Anal. Found (%): C, 39.2; H, 3.2; N, 8.7. Calcd for $C_{32}H_{32}F_{12}N_6O_5P_2Ru$ (%): C, 39.6; H, 3.3; N, 8.7. IR bands (KBr, ν/cm^{-1}): 3083 w, 1730 w, 1617 s, 1604 s, 1467 s, 1424 w, 1235 s, 1142 w, 845 s, 762 w, 731 w. UV−vis spectrum (MeCN) [λ_{max} (nm), (ϵ_{max}) (M^{-1} cm^{-1})]: 243 (24 500), 252 (23 300), 286 (72 800), 422 (9300), 452 (12 000). ^{1}H NMR (CD_3CN): δ 8.95 (s, 1H), 8.52 (m, 5H), 8.03 (m, 4H), 7.73 (m, 5H), 7.64 (d, 1H, ^3J = 5.7 Hz), 7.51 (d, 1H, ^3J = 5.8 Hz), 7.38 (m, 4H), 7.19 (dd, 1H, ^3J = 5.8 Hz, ^4J = 1.0 Hz), 2.51 (s, 3H). Electrospray mass spectrum (*m*/*z*) (positive mode): 314 [$(Ru(bpy)_2(Mebpy\text{-}COOH)^{2+}$, (M^{2+})], 627 [$(Ru(bpy)_2(Mebpy\text{-}COO)^+$, $(M-H)^+$].

Bis(1,10-phenanthroline)(4′-methyl-2,2′-bipyridine-4-carboxylic acid)ruthenium(II) Perchlorate] pentahydrate, $[Ru(phen)_2(Mebpy\text{-}COOH)](ClO_4)_2\cdot 5H_2O$ (2). This complex was prepared in the same manner as $[Ru(bpy)_2(Mebpy\text{-}COOH)](PF_6)_2\cdot 3H_2O$(**1**), but $[Ru(Mebpy\text{-}COOH)(CO)_2Cl_2]\cdot H_2O$ (0.69 g, 1.6 mmol) and 1,-10-phenanthroline (0.53 g, 2.9 mmol) were used. The crude product was purified by column chromatography on silica gel (eluent MeCN/H_2O/aqueous saturated solution of KNO_3, 10:3:1 v/v). The darkest band was collected, and the solvent was removed under reduced pressure. The residue was suspended in MeCN to dissolve the complex and to separate it from the insoluble KNO_3. After

(44) Kissinger, T.; Heineman, W. R. In *Laboratory Techniques in Electroanalytical Chemistry*, 2nd ed;Fry, A. J., Ed; Marcel Dekker: New York, 1996; Chapter 15, pp 469−486.

(45) Wolfbauer, G.; Bond, A. M.; Deacon, G. B.; MacFarlane, D. R.; Spiccia, L. *J. Am. Chem. Soc.* **2000**, *122*, 130−142.

filtration, MeCN was removed via rotary evaporation, and the product was redissolved in 5 mL of water. A 2 M $NaClO_4$ solution was added dropwise, until no further precipitation was observed, to give a dark red solid. The crystals were collected by filtration, washed with ether, and dried under high vacuum to give **2** as a red solid (yield 0.46 g, 31%). Slow evaporation of an acetonitrile/water mixture containing **2** and $NaClO_4$ deposited crystals of **2a**, [Ru(phen)$_2$(Mebpy-COO)](ClO_4)·6H_2O (the deprotonated derivative of **2**), that were suitable for X-ray crystallography.

Characterization Data for 2. Anal. Found (%): C, 44.9; H, 3.2; N, 8.7. Calcd for $C_{36}H_{36}Cl_2N_6O_{15}Ru$ (%): C, 44.8; H, 3.8; N, 8.7. IR bands (KBr, ν/cm^{-1}): 3084 w, 2960 w, 2925 w, 1718 w, 1636 w, 1617 s, 1426 w, 1377 s, 1235 w, 1140s, 1086 s, 842 s, 722 w. UV−vis spectrum (MeCN) [λ_{max} (nm), (ϵ_{max}) (M^{-1} cm^{-1})]: 221 (38 600), 263 (54 200), 289 (24 700), 417 (8800), 451 (15 500). ^{1}H NMR (DMSO-d_6): δ 8.97 (s, 1H), 8.80 (d, 2H, ^3J = 5.9 Hz), 8.68−8.73 (m, 3H), 8.31−8.42 (m, 4H), 8.24 (ddd, 2H, ^3J = 4.7 Hz, ^4J = 1.1 Hz), 7.91−7.97 (m, 4H), 7.64−7.71 (m, 4H), 7.49 (d, 1H, ^3J = 5.8 Hz), 7.23 (dd, 1H, ^3J = 5.8 Hz, ^4J = 0.9 Hz), 2.51 (s, 3H). Electrospray mass spectrum (*m*/*z*) (positive mode): 338 [(Ru(phen)$_2$(Mebpy-COOH)$^{2+}$, (M^{2+})], 675 [(Ru(phen)$_2$(Mebpy-COO)]$^+$, (M − H)$^+$].

Bis(dipyrido [3,2,-a;2′,3-c] phenazine)(4′-methyl-2,2′-bipyridine-4-carboxylic acid)ruthenium(II) dichloride nonahydrate, [Ru(dppz)$_2$(Mebpy-COOH)]Cl$_2$·9H$_2$O (3). [Ru(Mebpy-COOH)(CO)$_2$Cl$_2$] (0.22 g, 0.5 mmol) and dipyrido[3,2,-a;2′,3-c]phenazine (0.29 g, 1.1 mmol) were dissolved in 25 mL of deoxygenated 2-methoxyethanol. An excess of Me_3NO (0.19 g, 2.5 mmol) was added to this solution, and the mixture was refluxed at 120 °C for 3 h. Removal of the 2-methoxyethanol solvent via rotary evaporation yielded a dark red solid. The solid was treated with acetone to dissolve any unreacted starting material. The undissolved solid was collected on a sinter funnel and washed thoroughly with another 10 mL portion of acetone. The dark red powder corresponding to the desired complex was dried under high vacuum (yield 0.30 g, 62%).

Characterization Data. Anal. Found (%): C, 51.8; H, 4.0; N, 12.5. Calcd for $C_{48}H_{48}Cl_2N_{10}O_{11}Ru$ (%): C, 51.8; H, 4.4; N, 12.6. IR bands (KBr, ν/cm^{-1}): 1718 m, 1686 w, 1618 s, 1542 m, 1419 s, 1358 s, 1234 w, 1078 w, 815 w, 764 s 727 s. UV−vis spectrum (MeCN) [λ_{max} (nm), (ϵ_{max}) (M^{-1} cm^{-1})]: 278 (94 000 est.), 355 (22 000 est.), 365 (22 000 est.), 440 (15000 est.). ^{1}H NMR (DMSO-d_6): δ 9.68 (dd, 2H, ^3J = 5.8 Hz, ^4J = 1.1 Hz), 9.59 (dd, 2H, ^3J = 5.8 Hz, ^4J = 1.0 Hz), 9.00 (s, 1H), 8.92 (s, 1H), 8.50−8.61 (m, 4H), 8.34 (dd, 2H, ^3J = 5.7 Hz), 8.25 (m, 2H), 8.18−8.21 (m, 4H), 8.04−8.10 (m, 2H), 7.85−7.89 (m, 3H), 7.68 (d, 2H, ^3J = 5.6 Hz), 7.27 (d, 1H, ^3J = 5.6 Hz), 2.51 (s, 3H). Electrospray mass spectrum (*m*/*z*) (positive mode): 440 [(Ru(dppz)$_2$(Mebpy-COOH)$^{2+}$, (M)$^{2+}$], 879 [(Ru(dppz)$_2$(Mebpy-COO)]$^+$, (M − H)$^+$].

***cis*-Carbonylchloro-(2,2′-bipyridine)(4′-methyl-2,2′-bipyridine-4-carboxylic acid)ruthenium(II) hexafluorophosphate hydrate [Ru(bpy)(Mebpy-COOH)(CO)Cl](PF$_6$)·H$_2$O.** 4′-Methyl-2,2′-bipyridine-4-carboxylic acid (0.30 g, 1.37 mmol) was added to a solution of [Ru(bpy)(CO)Cl$_2$]$_2$ in deoxygenated 2-methoxyethanol (0.55 g, 1.2 mmol, 25 mL) under a N_2 atmosphere. This solution was refluxed at 120 °C for 2 h until a dark orange solution was formed. The solvent was removed in vacuo to yield a pale orange solid. This residue was suspended in distilled H_2O, sonicated for 5 min, and cooled to 4 °C, at which time any undissolved solid was removed by filtration. The filtrate was collected and mixed with a 1 M aqueous solution of KPF_6 (5 mL) to yield an orange solid. This solid was collected by filtration, washed once with H_2O, once with H_2O/EtOH (1:1 v/v), and dried at 70 °C in air (yield 0.62 g, 91%).

Characterization Data. Anal. Found (%): C, 39.9; H, 3.2; N, 8.0. Calcd for $C_{23}H_{20}ClF_6N_4O_4PRu$ (%): C, 39.6; H, 2.9; N, 8.0. IR bands (KBr, ν/cm^{-1}): 1974 s, 1719 s, 1623 m, 1560 w, 1471 w, 1449 w, 1411 w, 1376 w, 1313 w, 1238 w, 1072 w, 1031 w, 1025 w, 842 s, 770s, 732 w. ^{1}H NMR (acetone-d_6): δ 9.66 (d, 1H, ^3J = 5.5 Hz), 9.29 (d, 1H, ^3J = 5.7 Hz), 8.99 (s, 1H), 8.81 (m, 2H), 8.67 (m, 1H), 8.49 (ddd, 1H, ^3J = 7.9 Hz, ^4J = 1.3 Hz), 8.19 (ddd, 1H, ^3J = 7.9 Hz, ^4J = 1.3 Hz), 8.02 (m, 2H), 7.91 (d, 1H, ^3J = 5.3 Hz), 7.86 (d, 1H, ^3J = 5.5 Hz), 7.74 (d, 1H, ^3J = 5.3 Hz), 7.44 (m, 1H), 2.71 (s, 3H). Electrospray mass spectrum (*m*/*z*): 535 [(Ru(bpy)(Mebpy-COOH)(CO)Cl)$^+$, (M$^+$)].

(2,2′-Bipyridine)(dipyrido[3,2,-a;2′,3-c]phenazine)(4′-methyl-2,2′-bipyridine-4-carboxylic acid)ruthenium(II) hexafluorophosphate pentahydrate, [Ru(bpy)(dppz)(Mebpy-COOH)](PF$_6$)$_2$·5H$_2$O (4). Dipyrido[3,2,-a;2′,3-c]phenazine (0.14 g, 0.50 mmol) and excess Me_3NO (0.50 g, 0.80 mmol) were added to a solution of [Ru(bpy)(Mebpy-COOH)(CO)Cl](PF$_6$)·H_2O in deoxygenated 2-methoxyethanol (25 mL) under a N_2 atmosphere. The round-bottom flask was covered with aluminum foil, and the solution was refluxed at 120 °C for 3 h under N_2 in the dark. After it was cooled to room temperature, the resulting bright orange colored solid that had precipitated was collected by filtration and washed with H_2O, cold ethanol, and ether successively. The solvent was removed from the filtrate in vacuo to give a viscous red oil, which was suspended in H_2O (25 mL) and sonicated for 5 min. After it was cooled to 4 °C and filtered, a 1 M aqueous solution of KPF_6 was added dropwise to the filtrate until no further precipitation of the product was observed. The dark red precipitate was collected by filtration and washed with H_2O, cold ethanol, and ether in succession. Both the dark red precipitate and orange solids were purified by column chromatography on silica gel (eluent MeCN/H_2O/aqueous saturated solution of KNO_3, 10:3:1 v/v). The darkest band was collected; the solvent was removed under reduced pressure, and the resulting solid was dissolved in MeCN, separating it from the insoluble KNO_3. The solvent was removed on a rotary evaporator, and the solid was redissolved in water. A 1 M aqueous solution of KPF_6 was then added dropwise to the aqueous solution until no further precipitation was observed. The dark red microcrystals were collected by filtration and washed with ether (yield 0.13 g, 26%).

Characterization Data. Anal. Found (%): C, 42.6; H, 3.0; N, 9.6. Calcd for $C_{40}H_{38}F_{12}N_8O_7P_2Ru$ (%): C, 42.6; H, 3.4; N, 9.9. IR bands (KBr, ν/cm^{-1}): 3084 w, 1720 w, 1617 s, 1604 s, 1477 s, 1235 w, 1142 w, 845 s. UV−vis spectrum (MeCN) [λ_{max} (nm), (ϵ_{max}) (M^{-1} cm^{-1})]: 257 (30 300), 280 (55 500), 365 (10 800), 445 (10 000). ^{1}H NMR spectrum (DMSO-d_6): δ for major isomer 9.62 (dd, 2H, ^3J = 6.9 Hz, J = 1.1 Hz), 8.98 (s, 1H), 8.84 (m, 4H), 8.52 (dd, 2H, ^3J = 6.5 Hz, ^4J = 3.4 Hz), 8.16−8.28 (m, 6H), 8.09 (ddd, 1H, ^3J = 7.9 Hz, ^4J = 1.5 Hz), 7.97 (m, 2H), 7.79 (s, 1H), 7.73 (m, 2H), 7.54−7.59 (m, 2H), 7.37 (m, 1H), 2.57 (s, 3H). Electrospray mass spectrum (*m*/*z*) (positive mode): 388 [((Ru(bpy)(dppz)(Mebpy-COO)$^+$ + Na$^+$), (M + Na)$^{2+}$], 753 [(Ru(bpy)(dppz)(Mebpy-COO)$^+$, (M − H)$^+$].

X-ray Crystallography. Intensity data from crystals of **1a** (0.21 × 0.19 × 0.06 mm) and **2a** (0.10 × 0.08 × 0.06 mm) were measured at 123 K using Nonius Kappa CCD (**1a**) and a Bruker Apex 2 CCD (**2a**) X-ray diffractometers which were fitted with graphite-monochromated Mo Kα radiation (0.71073 Å). The data were collected to a maximum 2θ value of 50° and processed using the Nonius software (Bruker Apex 2 software for **2a**). Collection and refinement parameters are summarized in Table 1. The structures were solved using direct methods and expanded with standard Fourier routines using SHELX-97 software.[46] All hydrogens were placed in idealized positions, and all non-hydrogen atoms were refined anisotropically.

Table 1. Selected Single-Crystal X-ray Diffraction Data for Complexes **1a** and **2a**[a]

	1a	**2a**
empirical formula	$C_{32}H_{25}F_{10.5}N_6O_2P_{1.75}Ru$	$C_{36}H_{25}ClN_6O_{11}Ru$
M (g mol^{-1})	880.35	854.14
cryst syst	monoclinic	monoclinic
space group	$C2/c$	$C2/c$
a (Å)	53.402(11)	18.7207(7)
b (Å)	26.317(5)	19.7328(9)
c (Å)	12.682(3)	20.2842(10)
β (deg)	99.28(3)	93.771(2)
V (Å^3)	17590(6)	7477.0(6)
Z	4	4
T (K)	123(2)	123(2)
λ (Å)	0.71073	0.71073
D_c (g cm^{-3})	1.330	1.546
μ(Mo Kα) (mm^{-1})	0.497	0.562
no. data measured	62 595	29 824
unique data (R_{int})	15 348 (0.1225)	6530 (0.0470)
obsd data [$I > 2(\sigma)I$]	6627	6092
final R1, wR2 (obsd data)	0.0733[a], 0.1729[b]	0.0649[a], 0.1410[b]
final R1, wR2 (all data)	0.1599, 0.2061	0.0702, 0.1439
ρ_{min}, ρ_{max} (e Å^{-3})	−0.668, 0.741	−0.708, 0.930

[a] $R1 = \sum(|F_o| - |F_c|)/\sum|F_o|$. [b] $wR2 = [\sum w(|F_o| - |F_c|)^2/\sum F_o^2]^{1/2}$, where $w = [\sigma^2(F_o)]^{-1}$.

The Fourier difference map for **1a** showed many peaks that would correspond to a high degree of disorder for the waters of cocrystallization. According to the microanalysis, there are three waters, and thus, the residual electron densities were eliminated using the PLATON SQUEEZE command.[47] The remaining electron density was calculated to 7.4 waters per asymmetric unit. This higher value is attributed to the hygroscopic nature of the compound. There was also disorder about one of the PF_6 anions, and the site occupancy of the fluorine atoms were modeled accordingly. The perchlorate anion in **2a** was disordered across two positions, and their site occupancies were refined against each other.

Results and Discussion

Synthesis and Solid-State Characterization. The synthesis of the ruthenium(II) complexes is described in Scheme 2. The starting material for the synthesis, the Ru^{II}-carbonyl chloride polymer, $[Ru(CO)_2Cl_2]_n$, has previously been used to prepare a variety of Ru^{II} diimine complexes.[9] With this synthon, the sequential addition of up to three dissimilar diimine ligands is achieved in good yield, and the final products are usually obtained in high purity. To the present time, however, this route has not been used to prepare complexes of diimine ligands incorporating carboxylic acid functional groups which, as indicated earlier, need to be introduced for applications, such as DSSCs and bioconjugates.[2,4,5,16] In this work, 4′-methyl-2,2′-bipyridine-4-carboxylic acid, Mebpy-COOH, has been introduced by reaction in an alcohol solvent. In the case of $[Ru(bpy)_2(Mebpy\text{-}COOH)]^{2+}$ (**1**), $[Ru(phen)_2(Mebpy\text{-}COOH)]^{2+}$ (**2**), and $[Ru(dppz)_2(Mebpy\text{-}COOH)]^{2+}$ (**3**), Mebpy-COOH is reacted with $[Ru(CO)_2Cl_2]_n$ to form $[Ru(Mebpy\text{-}COOH)(CO)_2Cl_2]$, which is then reacted with 2 equiv of bpy or phen in the presence of the decarbonylating agent, Me_3NO, to form the complexes. Single crystals of **1a** and **2a** suitable for X-ray diffraction were grown by slow evaporation of the dissolved complex. The synthesis of $[Ru(bpy)(dppz)(Mebpy\text{-}COOH)]^{2+}$ (**4**), involved the sequential addition of bpy, Mebpy-COOH, and finally, dppz in the presence of Me_3NO (Scheme 2).

All of the Ru^{II} compounds synthesized were characterized using ^{1}H NMR, electrospray mass, and IR spectroscopy and elemental analysis (see Experimental Section). The positive ion mass spectra of **1**−**4** showed peaks corresponding to the protonated complex cation $[(M)^{2+}]$ and deprotonated cation $[(M)^{1+}]$ at $m/z = 314$ and 627 for **1**, $m/z = 338$ and 675 for **2**, and $m/z = 440$ and 879. For **4**, significant peaks were found at $[M(\text{deprotonated}) + Na]^{2+} = 388$ and $[M(\text{deprotonated})]^{+} = 753$ for **4**. Elemental analysis indicated that the complexes contain a number of waters of solvation. Furthermore, the microanalysis of **2** revealed that the bulk material consisted of the protonated form of **2**. However, the crystals used in the X-ray structure determination, obtained by crystallization from an aqueous solution of **2** and sodium perchlorate, were of the deprotonated complex, $[Ru(phen)_2(Mebpy\text{-}COO)]^{+}$, **2a**. The IR spectrum of each complex showed vibrations caused by asymmetric stretching of the protonated carboxylate group (ν_{asym} at 1730, 1721, 1718, and 1720 cm^{-1} for **1**, **2**, **3**, and **4**, respectively), but the symmetric carboxylate stretching mode typically found near 1400 cm^{-1} was masked by other vibrations in this region.

X-ray Crystal Structure Determinations. The X-ray crystal structures of **1a** and **2a** are shown in Figures 2 and 3 with crystal data and selected bond lengths and angles given in Tables 1 and 2, respectively. The asymmetric unit (ASU) of **1a** contains two octahedral $[Ru(bpy)_2(Mebpy\text{-}COOH)]^{2+}$ cations whose charge is balanced by 3.5 $[PF_6]^-$ anions (one of which lies on a special position), suggesting that across the whole crystal system one in four cations contains a deprotonated carboxylate group.

The ruthenium(II) centers in **1a** adopts a distorted octahedral geometry, as indicated by *cis*-N−Ru−N chelate angles below 90° and typical of 5-membered chelate rings formed by bipyridine ligands (see Table 2). The Ru−N bond lengths, 2.056(7)−2.077(5) Å, are consistent with those observed previously for Ru^{II} complexes of bipyridine carboxylates and bipyridines in general.[48] The location of the atoms of the carboxylate group is poorly defined; the C−O bond lengths and O−C−O bond angles in **1** are subject to large errors (1.26(1)−1.27(1) Å and 127(1)°, respectively), but these parameters correspond well to those reported by Caspar et al. (1.21(1)−1.25(1) Å and 124.7(10)−126.6(8)°).[49,50]

The crystal structure of **1a** reveals $\pi^*\cdots\pi$ interactions between the substituted bipyridine rings and an alternating $\pi\cdots\pi$ interaction between the unsubstituted bipyridine on

(46) Sheldrick, G. M. *SHELXS-97*; University of Göttingen: Göttingen, Germany, 1997.
(47) Spek, A. L. *J. Appl. Crystallogr.* **2003**, *36*, 7−13.
(48) Eskelinen, E.; Luukkanen, S.; Haukka, M.; Ahlgren, M.; Pakkanen, T. A. *J. Chem. Soc., Dalton Trans.* **2000**, *16*, 2745−2752.
(49) Caspar, R.; Musatkina, L.; Tatosyan, A.; Amouri, H.; Gruselle, M.; Cordier, C.; Guayard-Dhayon, C.; Duval, R. *Inorg. Chem.* **2004**, *43*, 7986−7993.
(50) Caspar, R.; Amouri, H.; Gruselle, M.; Cordier, C.; Malezieux, B.; Duval, R.; Leveque, H. *Eur. J. Inorg. Chem.* **2003**, *3*, 499−505.

Scheme 2. Synthesis of **1**−**4**[a]

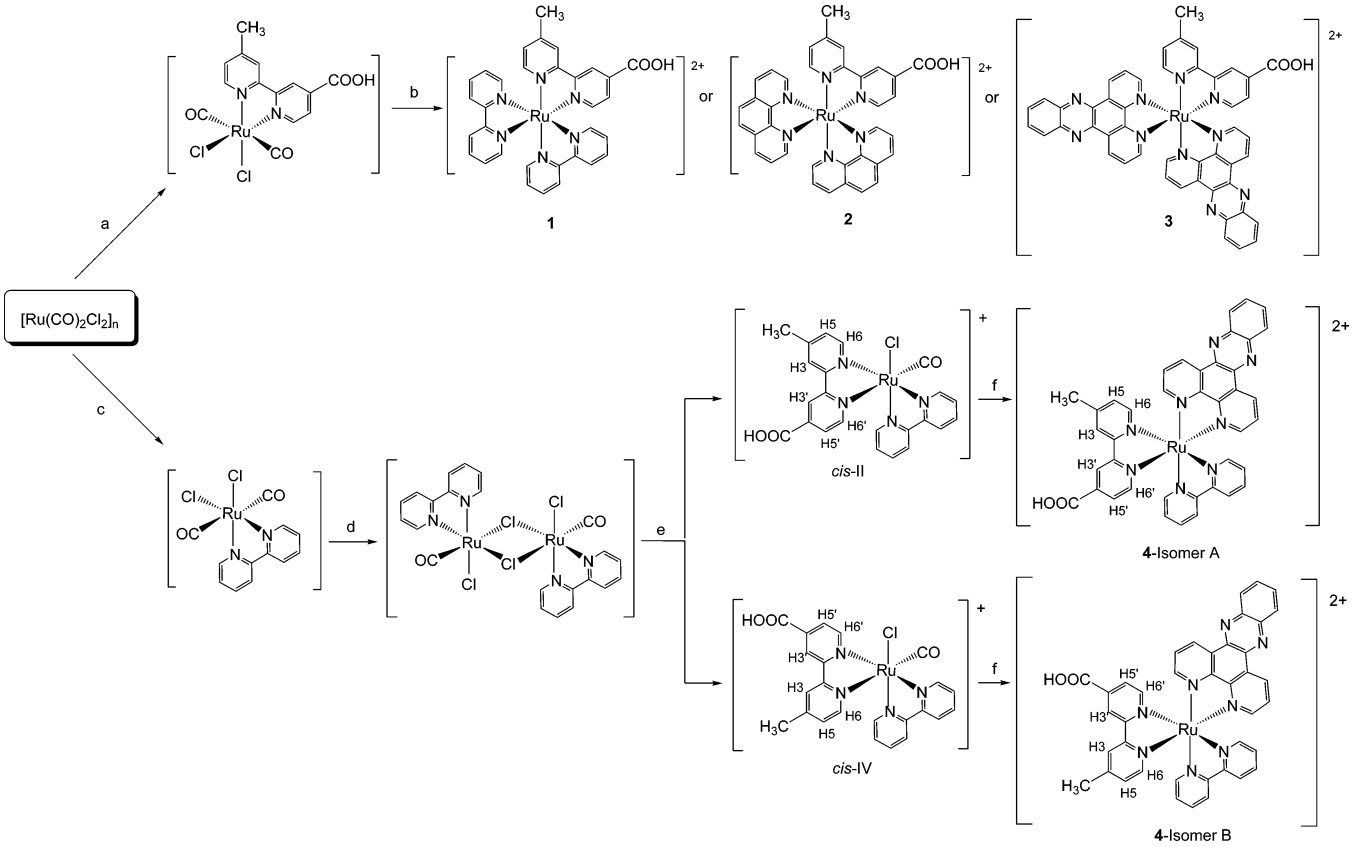

[a] (a) Mebpy-COOH, methanol, reflux, 20 min; (b) 2 equiv of bpy, phen, or dppz, excess Me_3NO, 2-methoxyethanol, reflux, 3 h; (c) bpy, methanol, reflux, 20 min; (d) *hν* light, dichloromethane, 48 h; (e) Mebpy-COOH, 2-methoxyethanol, reflux, 2 h; (f) dppz, excess Me_3NO, 2-methoxyethanol, reflux, 3 h.

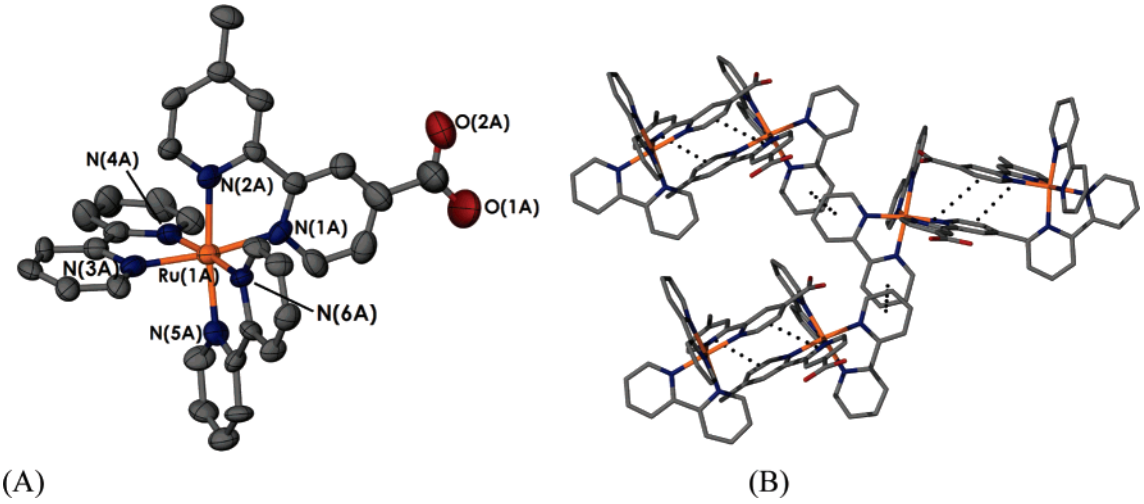

Figure 2. (A) Thermal ellipsoid plot of a single cationic unit of **1a.** Probability ellipsoids drawn at 50%, and hydrogen atoms omitted for clarity. (B) $\pi\cdots\pi$ interactions in **1a** (represented by dashed bonds).

adjacent cations that links up the complex cations in an infinite array (Figure 2(B)).

The asymmetric unit of compound **2a** consists of an octahedral $[Ru(phen)_2(Mebpy\text{-}COO)]^+$ cation (Δ enantiomer, the other enantiomer generated by symmetry), a disordered $[ClO_4]^-$ anion, and six H_2O molecules (one of which is disordered across two positions). The structural parameters for the RuN_6 core and the carboxylate pendants match closely to those of **1a**. An interesting feature in the structure of **2a** (shown in Figure 3B) is the presence of π-stacking between the phen ligands on adjacent molecules, as well as the $\pi^*\cdots\pi$ bonds, with plane-to-plane distances of 3.935(4) and 3.619(4) Å, respectively. This binding motif forms a repeating infinite linear chain linking up adjacent complex cations.

Solution ^{1}H NMR Spectroscopy. ^{1}H NMR assignments of complexes **1**−**4** were complicated by the presence of protonated and deprotonated forms of complexes in solution. ^{1}H−^{1}H COSY spectra of **1**−**4** were measured to assist with these assignments (see Figures S1−S6, Supporting Information). In the case of **4**, the asymmetric nature of the Mebpy-

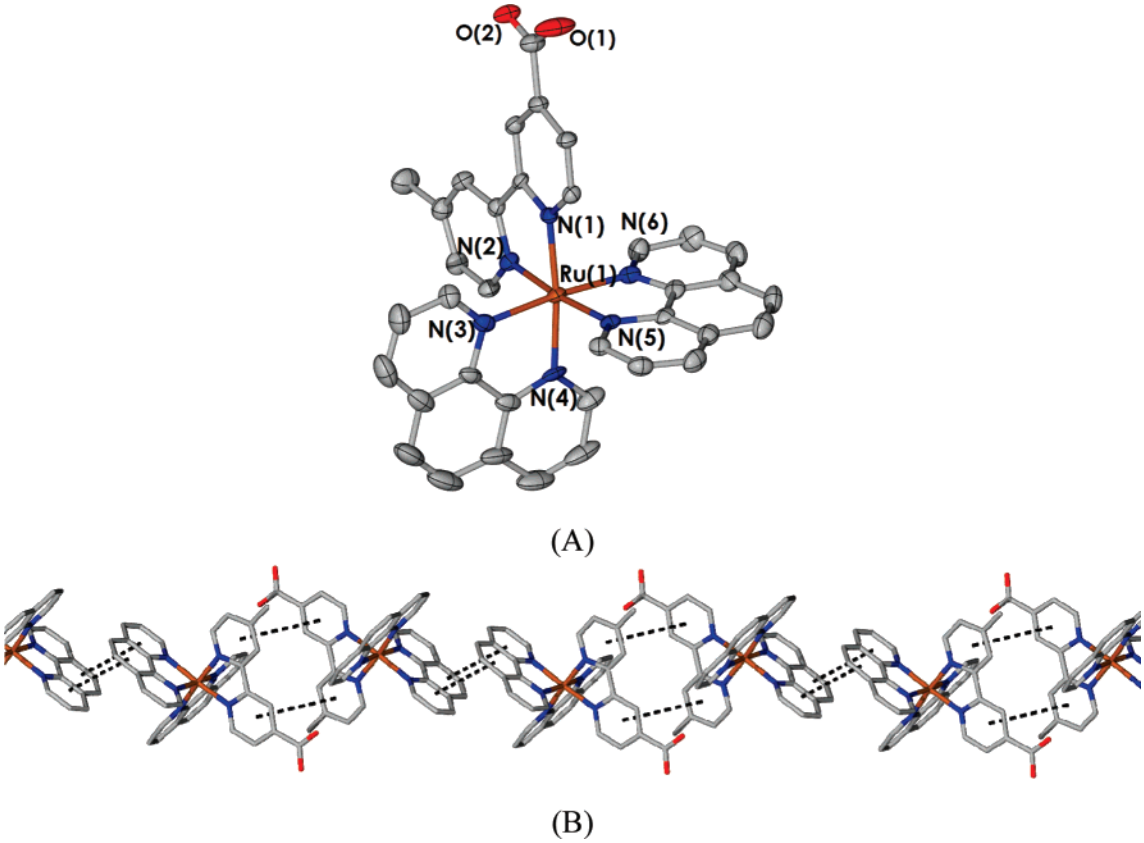

Figure 3. (A) Thermal ellipsoid plot of **2a**. Thermal ellipsoids drawn at 50%. Hydrogen atoms, counteranions, and water omitted for clarity. (B) $\pi-\pi$ interactions of **2a**, showing a 1-dimensional infinite linear chain being formed.

Table 2. Selected Bond Lengths (Å) and Angles (deg) for Complexes **1a** and **2a**[a]

1a		**2a**	
Ru(1A)−N(1A)	2.051(6)	Ru(1)−N(1)	2.047(4)
Ru(1A)−N(3A)	2.056(7)	Ru(1)−N(2)	2.041(4)
Ru(1A)−N(2A)	2.059(5)	Ru(1)−N(3)	2.073(5)
Ru(1A)−N(4A)	2.066(6)	Ru(1)−N(4)	2.061(4)
Ru(1A)−N(5A)	2.076(5)	Ru(1)−N(5)	2.063(4)
Ru(1A)−N(6A)	2.076(5)	Ru(1)−N(6)	2.049(4)
O(1A)−C(31A)	1.27(1)	C(11)−O(1)	1.253(7)
O(2A)−C(31A)	1.26(1)	C(11)−O(2)	1.236(7)
N(1A)−Ru(1A)−N(2A)	78.1(2)	N(2)−Ru1−N(1)	79.0(2)
N(3A)−Ru(1A)−N(4A)	79.0(3)	N(6)−Ru1−N(5)	79.9(2)
N(5A)−Ru(1A)−N(6A)	79.1(2)	N(4)−Ru1−N(3)	79.8(2)
N(1A)−Ru(1A)−N(3A)	172.3(2)	N(1)−Ru(1)−N(4)	173.14(2)
N(2A)−Ru(1A)−N(5A)	172.8(2)	N(2)−Ru(1)−N(5)	173.80(2)
N(4A)−Ru(1A)−N(6A)	174.6(2)	N(6)−Ru(1)−N(3)	174.54(2)
N(1A)−Ru(1A)−N(5A)	97.6(2)	N(1)−Ru(1)−N(6)	89.26(2)
N(3A)−Ru(1A)−N(5A)	89.3(2)	N(6)−Ru(1)−N(4)	95.23(2)
O(2A)−C(31A)−O(1A)	127(1)	O(2)−C(11)−O(1)	126.1(5)

[a] esd in parenthesis.

COOH ligand can lead to two geometric isomers, A and B, which have the carboxylate group trans to either bpy or dppz (Scheme 2). Attempts to separate these geometric isomers following the method of Keene et al. proved unsuccessful.[51] The ^{1}H NMR spectra measured before and after cation exchange column chromatography were the same. The isomeric ratio for **4** was found to be 1:4 with the major isomer being assigned as isomer A from Scheme 2, following identification of the major isomer in the precursor to this complex as *cis*-II/[Ru(bpy)(Mebpy-COOH)(CO)Cl](PF$_6$) (Figure 4).

The asymmetric nature of [Ru(bpy)(Mebpy-COOH)(CO)Cl](PF$_6$) leads to five possible geometric isomers, of which, four assume the *cis* configuration as shown in Figure 4. The presence of three geometric isomers in the crude product, [Ru(bpy)(Mebpy-COOH)(CO)Cl](PF$_6$) was established via ^{1}H NMR spectroscopy, which exhibited three methyl resonances at 2.46 (minor), 2.54 (major), and 2.76 ppm (minor). Peak integration was used to establish that 75% of the crude product comprises the major isomer. In determining the conformation of the major isomer, we note that [Ru(bpy)(Mebpy-COOH)(CO)Cl](PF$_6$) was prepared from the dimer, [Ru(bpy)(CO)Cl$_2$]$_2$, the cleavage of which produces the *cis* and *trans* isomers, specifically *cis*-II, *cis*-IV, and *trans*-V (Scheme 2 and Figure 4). The formation of the *cis*-I and *cis*-III isomers is unlikely because it would require a prearrangement through dissociation of the ligands.

For the major isomer observed in the ^{1}H NMR spectrum, the H3 proton adjacent to the COOH moiety appears at 8.99 ppm, whereas the H3′ proton next to the CH$_3$ group is identified at 8.79 ppm. Analysis of the COSY spectrum indicates that the H6′ resonance meta to the methyl group of the functionalized bpy appears at 9.29 ppm, in contrast to the H6 meta to the carboxylate moiety appearing at 7.88 ppm. This suggests that shielding of the COOH-attached pyridyl ring protons is caused by the neighboring bipyridine

(51) Rutherford, T. J.; Pellegrini, P. A.; Aldrich-Wright, J.; Junk, P. C.; Keene, F. R. *Eur. J. Inorg. Chem.* **1998**, *11*, 1677−1688.

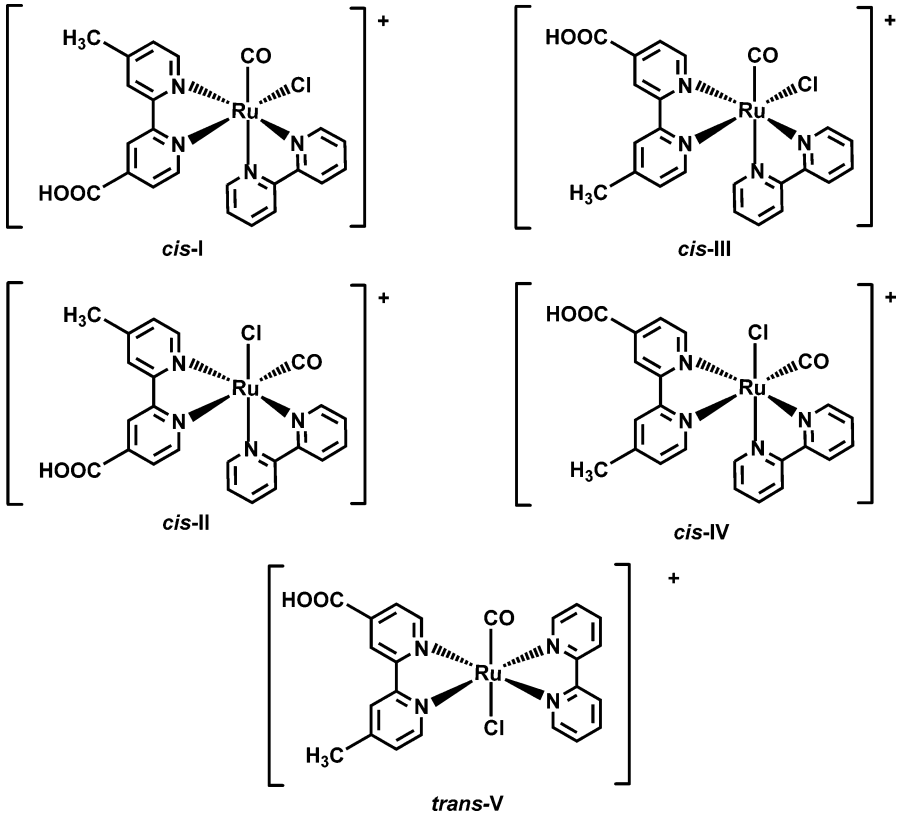

Figure 4. Possible isomers of [Ru(bpy)(Mebpy-COOH)(CO)Cl](PF_6).

ring and vice versa; the CH_3 pyridyl ring protons are free from any shielding effects, particularly allowing H3′ and H6′ protons of this particular ring to resonate farthest downfield. Thus, the deshielding of the H3′ and H6′ protons confirms that the major isomer formed is in the *cis*-II configuration, dominating over the *cis*-IV and *trans*-V configuration. Given that the major isomer of complex **4** is derived from the *cis*-II configuration of the precursor, the major isomer of **4** can be deduced to be isomer A. The assignment of the ^{1}H NMR resonances in **4**, $[Ru(bpy)(dppz)(Mebpy\text{-}COOH)]^{2+}$, was further aided by the assignments of the ^{1}H NMR spectrum of $[(bpy)_2Ru(tpphz)Ru(bpy)(dcb^{-})]^{3+}$ (tppzh = tetrapyrido-[3,2-a:2′,3′-c:3″,2″-h:2‴,3‴-j]phenazine) reported by Gholamkhass et al.[52]

Electronic Spectroscopy and Electrochemistry. General Comments. UV−vis spectrophotometry, emission spectroscopy, and electrochemical studies of **1**−**4** were conducted in MeCN. All complexes were found to be solvated by water and retained H_2O molecules even after drying under high vacuum at 130 °C, as observed in the microanalysis and in the case of **1**, by the ^{1}H NMR spectrum recorded in an aprotic solvent (MeCN). On dissolution, the presence of small amounts of water in the isolated complexes can influence the degree of protonation/deprotonation of the carboxylate group attached to one bipyridine, causing shifts in the equilibrium. Notably, the pK_a of $[Ru(bpy)_2(H_2dcbpy)]^{2+}$ (H_2-dcbpy = 2,2′-bipyridine-4,4′- dicarboxylic acid), 1.75 in aqueous medium (eq 1),[53] indicates that this compound is moderately acidic.

$$[Ru(bpy)_2(H_2dcbpy)]^{2+} \rightleftharpoons [Ru(bpy)_2(Hdcbpy)]^{+} + H^{+} \quad (1)$$

$$[Ru(L)(L')(Mebpy\text{-}COOH)]^{2+} \rightleftharpoons [Ru(L)(L')(Mebpy\text{-}COO)]^{+} + H^{+} \quad (2)$$

For compounds **1**−**4**, the corresponding equilibrium is given by eq 2 (L = L′ or L ≠ L′). For these compounds, excess trifluoroacetic acid (TFA) and triethylamine (TEA) were added to the MeCN solutions of the complexes to generate solutions that predominantly contain the complex with the protonated or deprotonated carboxylate functionalities, respectively. The spectral data obtained for these solutions were used to assist in the analysis of the photochemical and electrochemical data.

The spectroscopic and electrochemical studies of compound **3** were complicated by the sparingly soluble nature of **3**, and therefore, the concentration of **3** in MeCN was not accurately known. In the case of **4**, two predominant geometric isomers with 75% of isomer A and 25% of isomer B (see earlier NMR discussion and Scheme 2) were identified but could not be separated. The electrochemistry and electronic spectroscopy are assumed to reflect predominately the properties of the major isomer A.

(52) Gholamkhass, B.; Hori, H.; Koike, K.; Negishi, N.; Sano, T.; Takeuchi, K. *Inorg. Chem.* **2003**, *42*, 2919−2932.

(53) Nazeeruddin, M. K.; Kalyanasundaram, K. *Inorg. Chem.* **1989**, *28*, 4251−4259.

Electronic Absorption Spectra. The UV−vis spectra of complexes **1**−**4** and $[Ru(bpy)_3]^{2+}$, measured (a) as dissolved, (b) in the presence of a 10-fold excess of TFA (fully protonated complex), and (c) in the presence of a 10-fold excess TEA (fully deprotonated complex), can be found in the Supporting Information (Figure S7). Spectral data is summarized in the Experimental Section. Consistent with previous studies, $[Ru(bpy)_3]^{2+}$ exhibits a band at 452 nm and a shoulder at 422 nm assigned to a MLCT (metal-to-ligand charge transfer, $d \rightarrow \pi^*$) transition,[54,55,56] which was unaffected by the addition of TEA and TFA. These MLCT transitions were also observed for complexes **1**−**4** in the dissolved, fully protonated, and deprotonated forms. The spectra of the as dissolved complexes in MeCN corresponded well to those observed on addition of TEA. This suggested that the isolated complexes were predominantly in the deprotonated form when dissolved in MeCN, that is, $[Ru(bpy)_2(Mebpy\text{-}COO)]^+$, $[Ru(phen)_2(Mebpy\text{-}COO)]^+$, or $Ru(bpy)(dppz)(Mebpy\text{-}COO)]^+$. In contrast to the situation with the spectrum of $[Ru(bpy)_3]^{2+}$, the addition of TFA causes a slight red shift in the absorption maximum of **1**−**4**, coupled with a significant broadening of the MLCT band toward the red region of the spectrum. An increase in molar extinction coefficient was observed, in agreement with the work of Kilsa et al.[57] The spectra of **1** and **2** are closely related to those of similar complexes, such as $[Ru(bpy)_2(dcbpy)]^{2+}$ and $[Ru(bpy)_2(bpy\text{-}COO)]^+$, where bpy-COO = 3-carboxy-2,2′-bipyridine, studied previously.[29,53,57−59] For $[Ru(bpy)_2(dcbpy)]$ and $[Ru(bpy)_2(bpy\text{-}COO)]^+$, broadening of the MLCT bands were also observed upon addition of acid, but were coupled to decreases in the intensities of the bands.[29,53,57,59] For **3** and **4**, an absorption band characteristic of the $\pi \rightarrow \pi^*$ transition of the planar dppz ligand was observed at 365 nm.[60,61]

Emission Spectroscopy. The emission spectra of **1**−**4** and $[(Ru(bpy)_3]^{2+}$ were recorded at 273 K in MeCN by exciting 10 μM solutions at 450 nm. The results are summarized in Figures 5 (protonated) and 6 (deprotonated) and Table S1. The as dissolved complexes, **1**, **2**, **3**, **4**, and $[Ru(bpy)_3]^{2+}$, show emissions at 623, 609, 630, 645, and 615 nm, respectively. The absorption maximum for $[Ru(bpy)_3]^{2+}$ of 615 nm is consistent with that reported by Balzani et al.[56]

The luminescence behavior of the as dissolved complexes, **1**−**4**, was similar to that observed upon addition of TEA, again confirming that the complexes were isolated as the deprotonated complexes. However, upon addition of TFA to ensure full protonation of the carboxylate group, significant red-shifts of 32 and 43 nm were observed for complexes **1** (655 nm) and **2** (652 nm). This indicates a decrease in the energy of the emission that could attributed to a lowering in the energy gap between the ^{3}MLCT excited-state and the ground state. Smaller shifts were observed for **3** (636 nm) and **4** (654 nm).

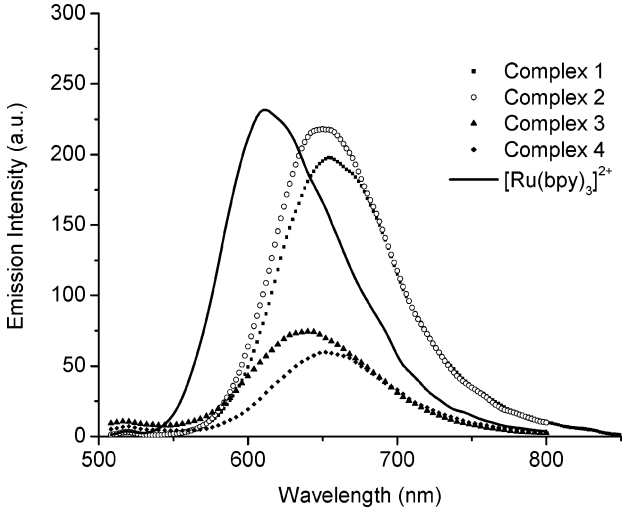

Figure 5. Emission spectra of 10 μM MeCN solutions of fully protonated (10 equiv of TFA added) **1**, **2**, **3**, and **4** in acetonitrile obtained from excitation at 450 nm.

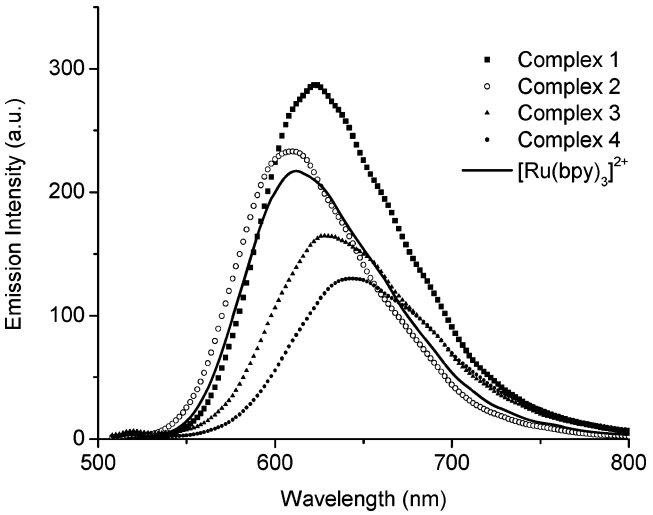

Figure 6. Emission spectra of 10 ±1 μM of MeCN solutions of fully deprotonated (10 equiv of TEA added) **1**, **2**, **3**, and **4** in acetonitrile obtained from excitation at 450 nm.

Significant shifts were observed upon protonation of $[Ru(bpy)_2(bpy\text{-}COO)]^+$ and $[Ru(bpy)_2(dcbpy)]$ in an aqueous medium,[29,53,55,58] and this behavior of Ru^{II} complexes incorporating carboxylate moieties has been previously rationalized in terms of proton-induced quenching of the triplet MLCT excited state via the promotion of nonradiative pathways. Notably, only a minor red-shift is observed upon addition of acid to $[Ru(bpy)_2(bpy\text{-}COO)]^+$ in a mixture of 2-methyltetrahydrofuran (2-MeTHF) and dichloromethane (DCM).[29] Such a solvent dependence (protic vs aprotic, dielectric constants, etc.) is derived from variations in the activity of the complex with solvent.

On the basis of the work of Zhou et al.,[26] the quantum yields, Φ_R, of complexes **1**−**4** were determined in MeCN

(54) Juris, A.; Balzani, V.; Belser, P.; Von Zelewsky, A. *Helv. Chim. Acta.* **1981**, *64*, 2175−2182.
(55) Cherry, W. R.; Henderson, L. J. *Inorg. Chem.* **1984**, *23*, 983−986.
(56) Balzani, V.; Barigelletti, S.; Belser, P.; Campagna, S.; Juris, A.; Von Zelewsky, A. *Coord. Chem. Rev.* **1988**, *84*, 85−277 and references therein.
(57) Kilsa, K.; Mayo, E. I.; Brunschwig, B. S.; Gray, H. B.; Lewis, N. S.; Winkler, J. R. *J. Phys. Chem.* **2004**, *108*, 15640−15651.
(58) Giordano, P. J.; Bock, C. R.; Wrighton, M. S.; Interrante, L. V.; Williams, R. F. X. *J. Am. Chem. Soc.* **1977**, *99*, 3187−3189.
(59) Ford, W. E.; Calvin, M. *Chem. Phys. Lett.* **1980**, *76*, 105−109.
(60) Ambroise, A.; Maiya, B. G. *Inorg. Chem.* **2000**, *39*, 4256−4263.
(61) Fees, J.; Kaim, W.; Moscherosch, M.; Klima, J.; Krejcik, M.; Zalis, S. *Inorg. Chem.* **1993**, *32*, 166−174.

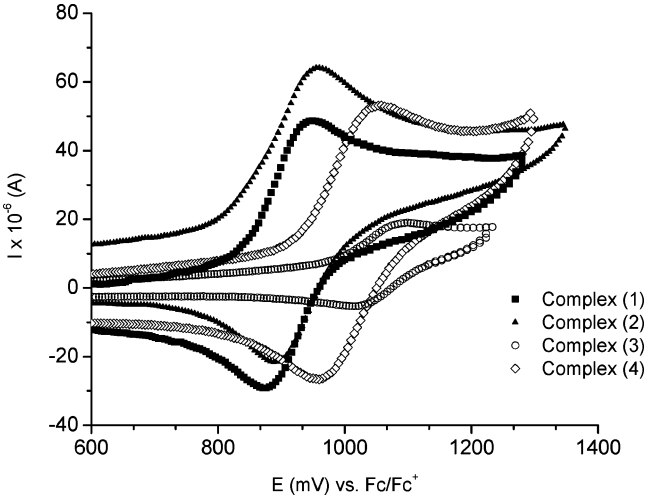

Figure 7. Comparison of cyclic voltammograms obtained at a Pt working electrode (0.0079 cm^2) using a scan rate of 100 mV s^{-1} for oxidation of **1** (1.01 mM), **2** (1.04 mM), **3** (saturated solution), and **4** (1.02 mM) in MeCN (0.1 M $^nBu_4NPF_6$).

assuming that Φ_{ref} of the reference compound, $[Ru(bpy)_3]^{2+}$, is 0.062. The quantum yield of the dissolved and fully deprotonated **1** is similar to that of $[Ru(bpy)_3]^{2+}$ and slightly higher than those for **2**−**4** (Table S1). The small differences in the quantum yields of dissolved and deprotonated **1**−**4** are consistent with the similar MLCT energies of the compounds. The addition of TFA decreases the quantum yields of **1**−**4** to varying degrees because of proton quenching effects.[29,53,55] The decrease in quantum yields is much greater for **3** and **4**, the two complexes bearing the dppz ligand, than for **1** and **2**.

Electrochemistry. Cyclic Voltammetry. The initial electrochemical characterization of **1**−**4** applied cyclic voltammetry to determine the midpoint potentials, E_m, associated with the Ru^{II}/Ru^{III} process over the scan rate range of 10−1000 mV s^{-1} (see Figure 7 for representative cyclic voltammograms and Table 3 for a summary of the data). For a reversible process, $E_m = E°_f$, the formal reversible potential for the Ru^{II}/Ru^{III} couple. Comparison was also made with the E_m value of 888 mV vs Fc/Fc^+ obtained for the $[Ru(bpy)_3]^{2+/3+}$ process. Voltammetric data obtained with a platinum working electrode are summarized in Table 3; similar data was obtained on as glassy carbon working electrode.

For the as-dissolved **1** and **2**, a close to reversible one-electron oxidation process is observed at all scan rates, but a small prewave also is detected at slow scan rates of ⩽100 mV s^{-1}. Cyclic voltammograms obtained over the scan rate range from 10 to 1000 mV s^{-1} are provided in Figure S8 and S9 (Supporting Information). For compound **1**, at slow scan rates, the prewave is detected at 700 mV, and the major reversible process is observed at 917 mV vs $Fc^{0/+}$. In the case of dissolved **2**, at scan rates of ⩽100 mV s^{-1}, the prewave appears at 857 mV, and the major reversible process is detected at 929 mV vs $Fc^{0/+}$. Dissolved **3** and **4** exhibit only a reversible one-electron oxidation process at all scan rates with E_m values at 1082 and 1042 mV vs $Fc^{0/+}$, respectively (see Figures S11 and S12, Supporting Information). A series of complicated ligand-based reduction steps were detected at negative potentials for each complex, but since only the metal based oxidation process is directly related to DSSC, biosensors, and other devices, detailed discussion presented herein is confined to the oxidation process.

Table 3. Cyclic Voltammetric Data Obtained at a Pt Working Electrode for Oxidation of **1** (1.03 mM), **2** (1.04 mM), **3** (Saturated Solution), and **4** (1.02 mM) in MeCN (0.1 M $^nBu_4NPF_6$) at (20 ± 2)°C

		irreversible process	reversible process				
	ν (mV s^{-1})	E_p^{ox} (mV)[a]	E_p^{ox} (mV)[a]	E_p^{red} (mV)[a]	ΔE_p (mV)[a]	E_m (mV)[a,b]	$\lvert i_p^{ox}/i_p^{red}\rvert$[c]
1	10	701	939	895	44	917	1.48
	20	700	942	887	55	915	1.31
	100	706	942	881	66	914	1.25
	500		971	867	102	917	1.24
	1000		973	888	110	917	1.24
2	10	857	950	898	52	924	0.80
	20	856	958	899	59	929	0.76
	100	859	960	894	66	927	0.78
	500		965	887	77	926	0.83
	1000		1070	881	88	925	0.83
3	20		1085	1022	63	1053	0.91
	100		1082	1016	66	1049	0.94
	200		1090	1015	75	1053	0.90
	1000		1082	1012	70	1047	0.92
4	20		1041	972	69	1007	1.05
	100		1042	967	75	1005	1.04
	200		1044	956	88	1000	1.02
	1000		1046	944	94	995	0.98
$[Ru(bpy)_3]^{2+}$	20		920	855	65	887	1.02
	100		919	854	65	887	0.98
	200		922	851	71	887	0.97
	1000		920	854	66	887	1.03

[a] Peak potentials are reported versus $Fc^{0/+}$ with an uncertainty of ±5 mV. [b] $E_m = (E_p^{ox} + E_p^{red})/2$, where E_p^{ox} and E_p^{red} are the oxidation and reduction peak potentials, respectively. [c] I_p^{ox}/I_p^{red} was calculated using the empirical method of Nicholson.[62]

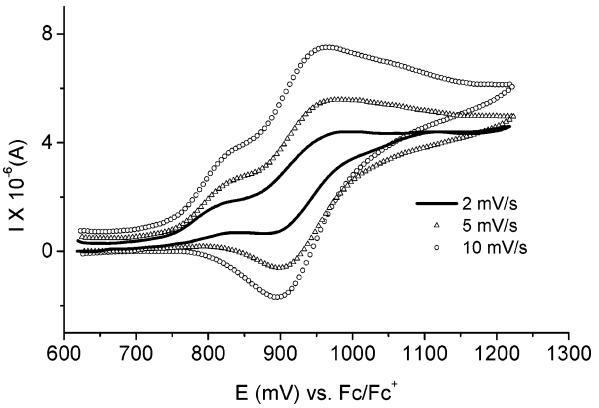

Figure 8. Comparison of cyclic voltammograms obtained at a Pt disc electrode (0.071 cm^2) using a range of slow scan rates from 2 to 10 mV s^{-1} for oxidation of 0.44 mM **2** using in MeCN (0.1 M $^nBu_4NPF_6$).

In the case of **1**, I_p^{ox} was not corrected for the prewave current, which is the origin of I_p^{ox}/I_p^{red} values larger than 1. In the case of **2**, the values of I_p^{ox} were corrected for the prewave contribution because better resolution of the two processes was available. Presentation of a detailed description of the electrochemistry of dissolved **2** facilitates the understanding of the electrochemical behavior of the series of compounds of interest in this paper. Cyclic voltammograms of **2** at even lower scan rates than those considered above (2−10 mV s^{-1}) allow resolution of the oxidation prewave and the major chemically reversible process (Figure 8). These data suggest that the irreversible prewave merges with the

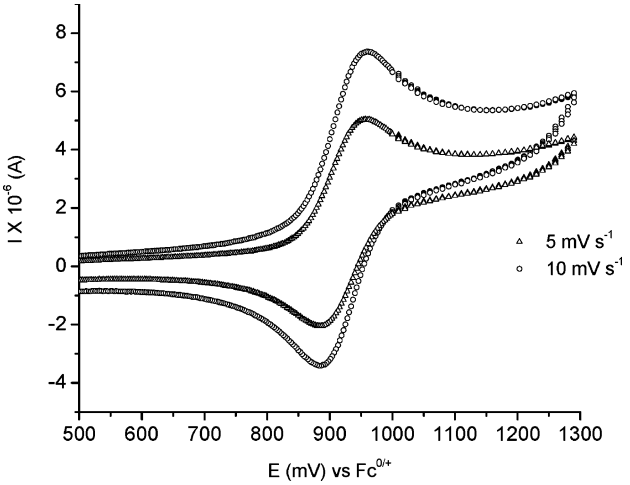

Figure 9. Cyclic voltammograms obtained at a Pt disc electrode (0.071 cm^2) using slow scan rates of 5 and 10 mV s^{-1} for oxidation of 0.44 mM **2** in the presence of 10 equiv of TFA in MeCN (0.1 M ^{n}Bu$_4$NPF$_6$).

second process at high scan rates, making its detection difficult under fast scan rate conditions.

The irreversible prewave may arise either from adsorption and oxidation of the carboxylate functionality on the Pt metal surface or from the oxidation of another species. To ascertain the likelihood that the chemical reaction was associated with the adsorption of the Ru^{II} complexes, cyclic voltammetry was repeated at a glassy carbon electrode, but a similar voltammetric response was observed, which suggests that surface interactions are not the origin of the prewave. ^{1}H NMR spectroscopy and microanalysis imply that **2** is pure, and thus, the prewave is unlikely to be associated with the oxidation of an impurity. However, the microanalysis of **2** reveals the presence of several water molecules, and therefore, voltammetric measurements on 1 mM concentrations of **2** were obtained in the presence of a significant concentration of water. It is therefore likely that the presence of two processes for **2** is associated with acid−base equilibria as shown in eq 3.

$$[Ru^{II}(phen)_2(Mebpy\text{-}COOH)]^{2+} + H_2O \rightleftharpoons [Ru^{II}(phen)_2(Mebpy\text{-}COO)]^{+} + H_3O^{+} \quad (3)$$

To determine if protonated and deprotonated forms of **2** are involved in the cyclic voltammetric behavior of **2**, 10 equiv of TFA was added to a 1 mM MeCN solution of **2** (0.1 M ^{n}Bu$_4$NPF$_6$). Cyclic voltammograms of the fully protonated **2**, obtained in the slow scan rate regime, used previously to clearly resolve the prewave and the major reversible wave, now exhibit only a reversible oxidation process with an E_m value of 922 mV, which is very close to the value obtained for the second reversible process found for **2** in the absence of acid (Figure 9). Thus, it is assumed that the protonated species gives rise to the reversible oxidation process shown in eq 4.

$$[Ru^{II}(phen)_2(Mebpy\text{-}COOH)]^{2+} \rightleftharpoons [Ru^{III}(phen)_2(Mebpy\text{-}COOH)]^{3+} + e^{-} \quad (4)$$

In the presence of acid, a plot of i_p^{ox} versus $\nu^{1/2}$ at the platinum electrode was linear, confirming via the Randles−Sevcik equation[63] that the process is now diffusion controlled (see Supporting Information), as would be expected for the Ru^{2+}/Ru^{3+} oxidation. The irreversible prewave is therefore considered to result from a kinetically controlled process associated with acid−base chemistry and oxidation of the deprotonated form of **2**, as expressed by eq 5a and b, where k_f and k_b are the rate constants for the forward (deprotonation) and reverse (protonation) reactions.

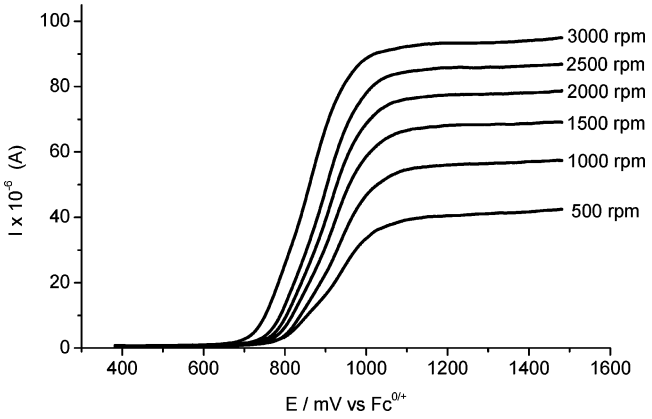

Figure 10. Platinum rotated disc electrode (0.071 cm^2) voltammograms obtained for 1.04 mM fully dissolved **2** in MeCN (0.1 M ^{n}Bu$_4$NPF$_6$) using a range of rotation rates from 500 to 3000 rpm at a scan rate of 10 mV s^{-1}.

$$[Ru^{II}(phen)_2(bpy\text{-}COOH)]^{2+} \underset{k_b}{\overset{k_f}{\rightleftharpoons}} [Ru^{III}(phen)_2(bpy\text{-}COO)]^{+} + H^{+} \quad (5a)$$

$$[Ru^{II}(phen)_2(bpy\text{-}COO)]^{2+} \rightleftharpoons [Ru^{III}(phen)_2(bpy\text{-}COO)]^{2+} + e^{-} \quad (5b)$$

In principle, the full reaction scheme involves a square scheme and two reversible potentials, E°_1 and E°_2 and, as summarized below, with water probably being the proton source.

$$\begin{array}{ccc} [(Ru^{II}(phen)_2(bpy\text{-}COO)]^{+} & \overset{E^o_1}{\rightleftharpoons} & [(Ru^{III}(phen)_2(bpy\text{-}COO)]^{2+} \\ -H^{+} \uparrow\downarrow H^{+} & & -H^{+} \uparrow\downarrow H^{+} \\ [(Ru^{II}(phen)_2(bpy\text{-}COOH)]^{2+} & \overset{E^o_2}{\rightleftharpoons} & [(Ru^{III}(phen)_2(bpy\text{-}COOH)]^{3+} \end{array}$$

Unfortunately, measurements in the presence of base (TEA) were not possible because TEA is oxidized at a potential that obscures the oxidation process assumed to be associated with the deprotonated form of **2**.

Rotated Disc Voltammetry. In the rotating platinum disc electrode voltammetry of dissolved **2**, investigated at rotation rates of 500−3000 rpm with a scan rate of 10 mV s^{-1}, two processes were detected with a significant dependence on electrode rotation being evident, as expected for a kinetically controlled process (Figure 10). Estimated $E_{1/2}$ values (potential where the current is half the value (I_L/2) of the limiting

(62) Nicholson, R. S. *Anal. Chem.* **1966**, *38*, 1406.
(63) Bard, A. J.; Faulkner, L. R. *Electrochemical Methods: Fundamentals and Applications*, 2nd ed.; John Wiley & Sons, Inc.: Brisbane, Australia, 2001.

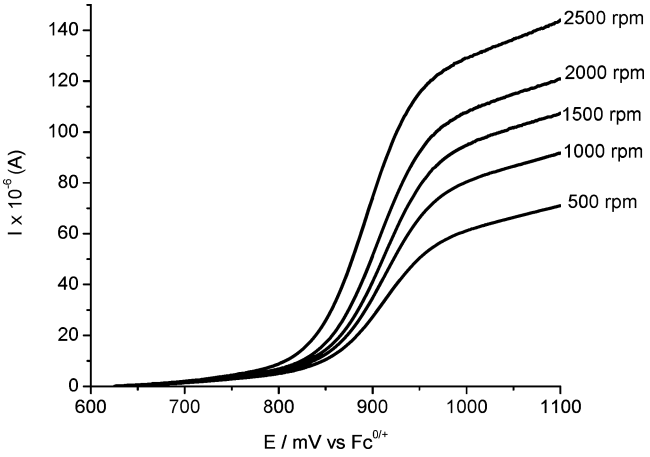

Figure 11. Platinum rotated disc electrode (0.071 cm^2) voltammograms obtained for 1.61 mM fully protonated **2** in MeCN (0.1 M $^nBu_4NPF_6$) using a range of rotation rates from 500 to 2500 rpm at a scan rate of 10 mV s^{-1}.

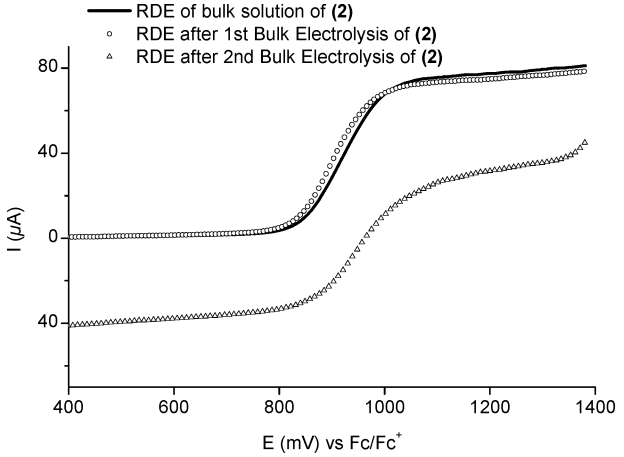

Figure 12. Platinum rotated disc electrode (0.0079 cm^2) voltammograms obtained for 1.04 mM of **2** before, after first bulk electrolysis at 815 mV vs $Fc^{0/+}$ and second bulk electrolysis at 900 mV vs $Fc^{0/+}$ in MeCN (0.1 M $^nBu_4NPF_6$) at a scan rate of 5 mV s^{-1}

current, I_L) are summarized in Table S2 (Supporting Information). The values, while containing considerable uncertainty caused by strong overlap of the two processes, lie in the same region as peaks located under conditions of cyclic voltammetry. The sum of the limiting currents for both processes is given in Table S2 and is linearly dependent on the square root of the rotation rate, as expected if the process controlled by mass transport in the positive potential region (Figure S10 Supporting Information). The Levich equation[64] aids in confirmation of the mass transport control of the reversible oxidation process, and its equation is

$$i_L = 0.620nFAD^{2/3}\omega^{1/2}\upsilon^{-1/6}C_0 \qquad (6)$$

where n is the number of electrons transferred ($n = 1$), F is Faraday's constant, A is the electrode area (cm^2), ω is the angular velocity of the electrode (s^{-1}), υ is the kinematic viscosity of the solvent ($\upsilon_{MeCN} = 0.0045$ cm^2 s^{-1}), C_0 is the bulk concentration (mol cm^{-3}), and D is the diffusion coefficient (cm^2 s^{-1}).

Upon addition of TFA, the rotated disc electrode voltammetry exhibits only a single oxidation process, as was the case with the cyclic voltammetry for the fully protonated form (Figure 11). The $E_{1/2}$ value of protonated **2**, 920 mV vs $Fc^{0/+}$, obtained at scan rates of $\leqslant$1500 rpm is close to the value for the reversible potential deduced from the cyclic voltammetry. However, at higher rotation rates, a small shift in $E_{1/2}$ to less-positive potentials indicates that a small level of kinetic control is still present (Figure 11).

Total limiting current obtained from the rotated disc electrode voltammetry and use of the Levich equation provided an estimate of the diffusion coefficient value of **2** of $(1.0 \pm 0.1) \times 10^{-5}$ cm^2 s^{-1} close to the reported diffusion coefficient value of 9.7×10^{-6} cm^2 s^{-1} for $Ru(bpy)_3^{2+}$ in MeCN.[65]

The rotated disc electrode voltammetry of complex **1** was also investigated at a rotating disc electrode in MeCN. Similar to **2**, a linear plot of I_L versus $\omega^{1/2}$ is obtained, and the diffusion coefficient for **1** was found from the Levich equation to be $(1.1 \pm 0.1) \times 10^{-5}$ cm^2 s^{-1}.

Bulk Electrolysis. The electrochemical behavior of dissolved **2** was also probed in MeCN by controlled potential electrolysis at a large surface area platinum gauze working electrode and potentials that corresponded to the oxidation of the first and the second process (815 and 900 mV vs Fc^+/Fc respectively). Analysis of the exhaustive electrolysis of 0.5−2 mM solutions, (complete within 30−50 min), implies that 0.20 ± 0.03 electrons per molecule are transferred in process 1 and 0.94 ± 0.06 electrons in process 2. This suggests that the overall oxidation process is slightly more than a one-electron step on long time scales. Voltammograms obtained from **2** after the first bulk electrolysis at 815 mV led to removal of the first process, so that only the second oxidation process remains at $E°_f = 920$ mV vs $Fc^{0/+}$ under conditions of cyclic voltammetry (Figure S13, Supporting Information). Thus, voltammograms are now similar to those obtained for **2** in the presence of TFA. This change in composition, observed after the first bulk electrolysis, was accompanied by changes in the UV−vis spectrum of **2** (Figure S14). Rotated disc electrode voltammograms after bulk electrolysis at the more positive potential became reductive, rather than oxidative (Figure 12), as expected if $[(Ru^{III}(phen)_2(bpy\text{-}COOH)]^{3+}$ is formed. However, if the potential was removed, slow spontaneous reconversion to an oxidation current occurs, implying reformation of $[(Ru^{II}(phen)_2(bpy\text{-}COOH)]^{2+}$.

Bulk electrolysis experiments are consistent with the reaction of Ru^{III} with H_2O leading to the protonated reduced product (eq 7). Thus, bulk electrolysis leads to an increase in acidity akin to the addition of TFA.

$$2[Ru^{III}(phen)_2(Mebpy\text{-}COOH)]^{3+} + 2H_2O \rightarrow 2[Ru^{II}(phen)_2(Mebpy\text{-}COOH)]^{2+} + 4H^+ + O_2 \qquad (7)$$

After bulk electrolysis at $E°_f = 900$ mV vs $Fc^{0/+}$, the UV−vis spectrum resembles that of a typical Ru^{III} complex.[66] The

(64) Levich, V. G. *Physicochemical Hydrodynamics*; Prentice Hall: Englewood Cliffs, NJ, 1962.
(65) McDevitt, M. R.; Addison, A. W. *Inorg. Chim. Acta.* **1993**, *204*, 141−146.
(66) Nazeeruddin, M. K.; Zakeeruddin, S. M.; Kalyanasundaram, K. *J. Phys. Chem.* **1993**, *97*, 9607−9612.

spectrum measured following conversion of the Ru^{III} complex to **2**, at a potential of 790 mV vs $Fc^{0/+}$, corresponded to that of the protonated complex obtained after bulk electrolysis of **2** at 815 mV vs $Fc^{0/+}$ (Figure S14).

As for **2**, the electrochemical behavior of complex **1** is affected by a mixture of deprotonated and protonated species in solution. Bulk electrolysis of complex **1** in MeCN at 740 and 860 mV vs Fc^{+}/Fc and coulometric analysis correspond to 0.04 ± 0.02 electrons per molecule being transferred during process 1 and 1.08 ± 0.03 electrons per molecule during process 2.

Complexes **3** and **4** exhibit only a single, reversible Ru^{II}/Ru^{III} couple with $E°_f$ values of 1005 and 1053 mV, respectively, at all scan rates and rotation rates. The small increase observed in ΔE_p with increasing scan rates for **4** can be attributed to uncompensated resistance. Unlike **1** and **2**, a prewave is not observed in **3** and **4**. Using the Randles−Sevcik equation, we determined the diffusion coefficient of **4** as $(8.7 \pm 0.1) \times 10^{-6}$ cm^2 s^{-1}.[63] Bulk electrolysis of **3** at 950 mV showed that 0.97 ± 0.06 electrons was transferred, and for **4**, at a controlled potential of 1000 mV, 1.08 ± 0.09 electrons was involved in the oxidation process. All data obtained from the bulk electrolysis are consistent with an overall one-electron oxidation Ru^{II}/Ru^{III} process.

Comparison of Reversible Potentials. The $E°_f$ values of **1**−**4** (protonated forms) are more positive than the $[Ru(bpy)_3]^{2+/3+}$ couple because of the electron-withdrawing properties of the carboxylate functionality. The $E°_f$ values of **1** and **2** are similar to each other but are less positive than for complexes **3** and **4** because of the high electron-accepting ability of the extended conjugated aromatic dppz systems. The additive effect of two dppz ligands in **3** compared to **4** induces a greater effect on the π-electron delocalization, and thus, the loss of an electron from the ruthenium(II) metal center of **3** becomes energetically more difficult, and hence, $E°_f$ occurs at a more-positive potential relative to that of **4**.

Conclusions

Three new complexes, $[Ru(phen)_2(bpy\text{-}COOH)]^{2+}$ (**2**), $[Ru(dppz)_2(bpy\text{-}COOH)]^{2+}$ (**3**), and $[Ru(bpy)(dppz)(bpy\text{-}COOH)]^{2+}$ (**4**), have been prepared together with $[Ru(bpy)_2(bpy\text{-}COOH)]^{2+}$ (**1**). The X-ray structures of **1a** and **2a** show high distortion in the octahedral geometry of the complexes and π-stacking between the aromatic rings of the functionalized ligands of complex **2a** was found. An electrochemical study in acetonitrile reveal the presence of a mixture deprotonated and protonated forms of **1** and **2**. The deprotonated forms of **1** and **2** give rise to an irreversible oxidation process prior to the chemically reversible couple associated with protonated forms in both the Ru^{II} and Ru^{III} redox states. All four complexes were also determined to be highly luminescent, except upon addition of acid, when the emission intensities of **3** and **4** decreased significantly, consequently affecting their quantum yields. Complex **1** showed the highest intensity in the luminescence (as dissolved, protonated, and deprotonated) compared to that of **2**−**4**. The degree of protonation of these complexes affects the emission maxima, UV−vis spectra, and the voltammetry of the Ru^{II}/Ru^{III} process.

Acknowledgment. We acknowledge financial support from the Australian Research Council through the Australian Centre for Electromaterials Science (L.S.) and the Discovery Program (A.M.B., G.B.D.). N.N. is the recipient of a Monash Departmental Scholarship, and M.J.B. is the recipient of an Australian Postgraduate Award.

Supporting Information Available: X-ray crystallographic files for **1a** and **2a** in CIF format, representative examples of the ^1H NMR and ^1H−^1H COSY spectra of complexes **2**−**4** (Figures S1−S6), electronic spectra (Figure S7−S8) and cyclic voltammograms of **1**−**4** as a function of scan rate (Figures S8−S9 and S11−S13), a Levich plot of the rotating disc voltammetry of **2** (Figure S10), electronic spectra following bulk electrolysis (Figure S14), and tables of electronic and emission spectroscopy data (Table S1) and platinum rotating disc voltammetric data for **2** (Table S2). This material is available free of charge via the Internet at http://pubs.acs.org.

IC700796M